universe

IMPACT FACTOR 2.9

CITESCORE 3.6

Article

QED Meson Description of the Anomalous Particles at ~17 and ~38 MeV

Cheuk-Yin Wong

Special Issue
Multiparticle Dynamics

Edited by
Prof. Dr. Tamás Csörgő, Prof. Dr. Máté Csanád and Dr. Tamás Novák

MDPI

https://doi.org/10.3390/universe10040173

universe

MDPI

Article

QED Meson Description of the Anomalous Particles at ∼17 and ∼38 MeV †

Cheuk-Yin Wong

Physics Division, Oak Ridge National Laboratory, Oak Ridge, TN 37831, USA; wongc@ornl.gov

† Based on a talk presented at the 52nd International Symposium on Multiparticle Dynamics, Gyöngyös, Hungary, 20–26 August 2023; Available online: https://indico.cern.ch/event/1258038/contributions/5538335/.

Abstract: The Schwinger confinement mechanism stipulates that a massless fermion and a massless antifermion are confined as a massive boson when they interact in the Abelian QED interaction in (1+1)D.If we approximate light quarks as massless and apply the Schwinger confinement mechanism to quarks, we can infer that a light quark and a light antiquark interacting in the Abelian QED interaction are confined as a QED meson in (1+1)D. Similarly, a light quark and a light antiquark interacting in the QCD interaction in the quasi-Abelian approximation will be confined as a QCD meson in (1+1)D. The QED and QCD mesons in (1+1)D can represent physical mesons in (3+1)D when the flux tube radius is properly taken into account. Such a theory leads to a reasonable description of the masses of π^0, η, and η', and its extrapolation to the unknown QED sector yields an isoscalar QED meson at about 17 MeV and an isovector QED meson at about 38 MeV. The observations of the anomalous soft photons, the hypothetical X17 particle, and the hypothetical E38 particle bear promising evidence for the possible existence of the QED mesons. Pending further confirmation, they hold important implications on the properties on the quarks and their interactions.

Keywords: quark confinement; QCD and QED; open-string model of QCD and QED mesons

Citation: Wong, C.-Y. QED Meson Description of the Anomalous Particles at ∼17 and ∼38 MeV. *Universe* **2024**, *10*, 173. https://doi.org/10.3390/universe10040173

Academic Editors: Máté Csanád and Tamás Novák

Received: 31 January 2024
Revised: 22 March 2024
Accepted: 28 March 2024
Published: 7 April 2024

1. Introduction

In the International Symposium on Multiparticle Dynamics in 2009 at Gomel, Belarus, Perepelitsa reviewed the phenomenon of the anomalous soft photons [1] and reported that in high-energy hadron–hadron [2–7] and e^+e^- collisions [1,8–10], anomalous soft photons in the form of excess e^+e^- pairs, are produced at a rate exceeding the standard model bremsstrahlung predictions by an average factor of about four. In particular, in exclusive DELPHI hadron production measurements in e^+e^- collisions at the Z^0 energy, the anomalous soft photons are proportionally produced whenever hadrons are produced, but they are not produced when hadrons are not produced [8,9]. The transverse momenta of the anomalous soft photons lie in the region of many tens of MeV/c, corresponding to the production of neutral bosons with masses in the region of many tens of MeV. Many different descriptions have been put forth to interpret the anomalous soft photons, including a cold quark gluon plasma [11–14], pion condensate [15], pion reflection [16], corrections to bremsstrahlung [17], color flux tube particle production [18], stochastic QCD vacuum [19,20], ADS/CFT supersymmetric Yang–Mills theory [21], Unruh radiation [22], closed quark–antiquark loop [23], QED-confined $q\bar{q}$ states [24–33], and induced currents in the Dirac sea [34].

It was soon realized [24] that the simultaneous and proportional production of the anomalous soft photons with hadrons suggests that a parent particle of an anomalous soft photon is likely to contain some elements of the hadron sector, such as a light quark and a light antiquark. Quarks and antiquarks carry color and electric charges, and they interact with the QCD and the QED interactions. The parent particle of an anomalous soft photon cannot arise from the light quark and the light antiquark interacting non-perturbatively in the QCD interaction because such a non-perturbative QCD interaction

will endow the pair with a mass much greater than the mass scale of the anomalous soft photons, in a contradictory manner. We are left only with the possibility of the quark and the antiquark interacting non-perturbatively in the QED interaction. Such a possibility is further reinforced by the special nature of attractive confining gauge interactions in which the smaller the coupling constant, the lower the mass of the confined composite particle. This is in contrast to non-confining attractive Coulomb-type or Yukawa-type interactions for which the smaller the coupling constant, the greater the mass of the composite system. Furthermore, the Schwinger confinement mechanism stipulates that a massless charged fermion interacting with an antifermion in a gauge field with the coupling constant g_{2D} in (1+1)D leads to a confined boson with a mass [35,36]

$$m_{\text{boson}} = \frac{g_{2D}}{\sqrt{\pi}}, \tag{1}$$

indicating that the mass of the confined fermion–antifermion composite system is directly proportional to the coupling constant. Application of the Schwinger confinement mechanism to quarks interacting in the QED interaction will bring the quantized masses of a $q\bar{q}$ pair to the lower mass region of the anomalous soft photons. It was therefore proposed in 2010 [24] that a light quark and a light antiquark interacting non-perturbatively with the QED interaction may lead to new open-string QED boson states (QED-meson states) with a mass of many tens of MeV. These QED mesons may be produced simultaneously with the QCD mesons in the string fragmentation process in high-energy collisions, and the excess e^+e^- pairs may arise from the decays of these QED mesons. For quarks with two flavors in the massless quark limit, the masses of the isoscalar and isovector QED mesons were predicted to be 12.8 MeV and 38.4 MeV, respectively (Table I of [24]).

In a series of experiments in search of axions, Krasznarhorkay and collaborators studied the e^+e^- spectrum in low-energy proton fusion of light α^n nuclei with n = 1, 2, and 3. Since 2016, they have been observing the occurrence of the hypothetical neutral "X17" boson with a mass of about 17 MeV from the e^+e^- spectrum (i) in the decay of the 18.15 MeV $I(J^\pi)$=0(1^+) excited ^{8}Be state to the ^{8}Be ground state [37], (ii) in the decay of the 18.05 MeV $I(J^\pi)$=0(0^-) excited ^{4}He state to the ^{4}He ground state [38,39], (iii) in the decay of the off-resonance excited ^{8}Be states to the ^{8}Be ground state [40], and (iv) in the decay of the 17.23 MeV $I(J^\pi)$=1(1^-) excited ^{12}C state to the ^{12}C ground state [41]. Updates of the ATOMKI measurements on the hypothetical X17 particle have also been presented [42–44]. In a recent measurement in the decay of the ^{8}Be 18.15 MeV state to the ^{8}Be ground state in the proton fusion on ^{7}Li, the Hanoi University of Science reported the observation of a significant structure, which indicates a hypothetical neutral boson with a mass of about 16.7 MeV decaying into e^+e^-, in support of the earlier ATOMKI observation [45]. An indirect support for the hypothetical X17 particle comes from the p_T spectrum of the anomalous soft photons in pp collisions at p_{lab}= 450 GeV/c [7], in the thermal model of the transverse momentum distribution [27,46].

The ATOMKI observation of the hypothetical X17 particle has generated a great deal of interest [24–32,42–71]. Although the mass of the hypothetical X17 particle was close to the isoscalar QED meson predicted earlier in [24], the X17 boson led to many speculations as discussed in the Proceedings of the Workshop on "Shedding lights on the X17" [42]. The proposed models include the QED meson [24–32], the axion [49], the fifth force of Nature [50], a dark photon [53], new physics particles [54], the Framed Standard Model [55–58], Higgs doublet [59], a 12-quark state [62], a light pseudoscalar [63], and dressed QED radiation [71]. The experimental confirmation of the hypothetical X17 particle is being actively pursued by many laboratories [42], including ATOMKI [43,44], HUS [45], Dubna [72], New JEDI [73], STAR [74], MEGII [75,76], ATLAS [77,78], CTU Prague [79,80], NTOF [81], NA64 [82], INFN-Rome [83], NA48 [84], Mu3e [85], MAGIX/DarkMESA [86], JLAB PAC50 [87,88], PADME [89,90], DarkLight [91,92], LUXE [93], FASER [94], ANU/UM [95], and Montreal [96].

In separate experiments, Abraamyan and collaborators at Dubna have been using the two-photon decay of a neutral boson to study the resonance structure of the lightest hadrons near their energy thresholds [97]. Upon the suggestion of van Beveran and Rupp [98–101], the Dubna Collaboration undertook a search for the E38 particle in d(2.0 GeV/n) + C, d(3.0 GeV/n) + Cu and p(4.6 GeV) + C reactions with internal targets at the JINR Nuclotron. They observed that the invariant masses of the two-photon distributions exhibit a resonance structure at around 38 MeV [102,103]. In a recent analysis in the diphoton spectrum in the lower invariant mass region, the Dubna Collaboration reported the observation of resonance-like structures both at ∼17 and ∼38 MeV [72], in support of the earlier ATOMKI observation of the hypothetical X17 particle and the earlier Dubna observation of the hypothetical E38 particle [102,103]. An indirect supporting signal for the hypothetical E38 particle comes from the p_T spectrum of anomalous soft photons in e^+e^- annihilations at the Z^0 resonance energy of $\sqrt{s} = 91.18$ GeV, which is consistent with the production of a neutral boson with a mass of about 38 MeV, in the thermal model of the transverse momentum distribution [27,46].

While there are many different theoretical interpretations, the open string $q\bar{q}$ QED meson model mentioned above [24,27] holds the prospect of describing the anomalous particles in a consistent framework. We would like to review here how such a model of QED and QCD mesons emerges as a reasonable theoretical concept consistent with experimental observations. We would also like to examine the implications for the existence of the QED mesons, if they are confirmed by future experimental measurements.

The cross-fertilization between condense matter physics and particle physics brings bountiful fruits on the physics frontiers. In this respect, it is worth pointing out that the confinement of electric charges and electric anticharges (Cooper pairs and anti-Cooper pairs in a specific case) in compact QED due to a linear potential (confining string) has been experimentally observed in condensed matter systems, where it gives rise to a new state of matter called super-insulators[1] (see [104–108]). There are similarities and also differences as one can surmise by comparing Figure 1 of ref. [104] and Figure 2b of ref. [33]. Whereas the confinement of QED mesons examined here is concerned with the QED confinement of massless fermions, the confinement of (charged boson)–(anticharged boson) in super-insulators in condenser matter physics is concerned with the QED confinement of massive bosons. The experimental existence of the QED super-insulators supports the possible existence of the QED mesons, which are good candidates for the X17 and E38 particles. Future parallel investigations on the common question of charge confinement in the QED interaction will bring benefits to both fields.

2. The Schwinger Confinement Mechanism

Schwinger showed in 1963 that a massless fermion and its antifermion interacting in the Abelian U(1) QED gauge interaction are bound and confined as a neutral QED boson with a mass [35,36] as given by Equation (1) where the coupling constant g_{2D} in (1+1)D has the dimension of a mass. Such a Schwinger confinement mechanism occurs for massless fermions interacting in Abelian U(1) gauge interactions of all strengths, including the interaction with a weak coupling (as in QED), as well as the interaction with a strong coupling (as in QCD in the quasi-Abelian QCD approximation, which we shall introduce below).

The masses of light quarks are about a few MeV [109,110]. Therefore, light quarks can be approximated as massless fermions, and we can apply the above Schwinger mechanism for massless fermions to quarks and antiquarks interacting in the QED interaction in (1+1)D. By such an application, we infer that a light quark and a light antiquark are bound and confined as a neutral QED boson in (1+1)D. From the works of Coleman, Jackiw, and Susskind [111,112], we can infer further that the Schwinger confinement mechanism persists even for massive quarks in (1+1)D.

It is instructive to review the Schwinger confinement mechanism here to understand how a light quark q and a light antiquark $\bar{q}$ approximated as massless can be confined in QED in (1+1)D. From the electrostatic viewpoint, the electric lines of force in (1+1)D

originate from the positive quark at x_q to end at the negative antiquark at $x_{\bar{q}}$, and the quarks experience a confining interaction [112]:

$$V_{q\bar{q}} = \frac{g_{2D}^2}{2}|x_q - x_{\bar{q}}|. \tag{2}$$

Such a confining interaction is one of the causes of quark confinement in (1+1)D. The spectrum of such a confining potential has been calculated in Appendix D of [28]. For light quarks which can be approximated as massless, there is an additional dynamical quark effect beyond the static linear interaction alone. The dynamics of quark matter current j^μ depends on the interacting gauge field A^μ, which in turn depends on the quark current j^μ in return, in an infinite loop of matter(j^μ)-and-field(A^μ) interaction that facilitates the confinement both of the matter field (j^μ) and the gauge field (A^μ). As a consequence, neither the quark field nor the gauge field make their external appearances, and there exists only a neutral massive boson field which emerges as free boson quanta containing both the quark field and the gauge field.

We consider the interacting quark–QED system as a quark–QED fluid and envisage the vacuum of the interacting quark–QED fluid as a calm Dirac sea with the lowest-energy state to consist of quarks filling up the (hidden) negative-energy Dirac sea and to interact with the QED interaction in (1+1)D space-time with coordinates $x = (x^0, x^1)$. The quark–QED vacuum is defined as the state that contains no valence quarks as particles above the Dirac sea and no valence antiquarks as holes below the Dirac sea. Subject to the applied disturbing gauge field $A^\mu(x)$ with a coupling constant g_{2D} in (1+1)D, the massless quark field $\psi(x)$ satisfies the Dirac equation,

$$\gamma_\mu[p^\mu - g_{2D}A^\mu(x)]\psi(x) = 0. \tag{3}$$

The applied gauge field $A^\mu(x)$ governs the motion of the quark field $\psi(x)$. From the motion of the quark field $\psi(x)$, we obtain the induced quark current $j^\mu(x) = \langle\bar{\psi}(x)\gamma^\mu\psi(x)\rangle$. If we consider only the sets of states and quark currents that obey the gauge invariance by imposing the Schwinger modification factor to ensure the gauge invariance of the quark Green's function, the quark current $j^\mu(x)$ at the space-time point x induced by the applied $A^\mu(x)$ can be evaluated. After the singularities from the left and from the right cancel each other, the gauge-invariant induced quark current $j^\mu(x)$ is found to relate explicitly to the applied QED gauge field $A^\mu(x)$ by [35,36,113]

$$j^\mu(x) = -\frac{g_{2D}}{\pi}\left(A^\mu(x) - \partial^\mu\frac{1}{\partial_\eta\partial^\eta}\partial_\nu A^\nu(x)\right). \tag{4}$$

We can understand the first term on the right-hand side of the above equation intuitively as indicating that the induced current gains in strength as the strength of the applied gauge field $A^\mu(x)$ increases, and it acquires a sign opposite to the sign of the applied gauge field $A^\mu(x)$ because an electric charge attracts charges of the opposite sign. The additional term on the right-hand side consists of the linear function of $A^\mu(x)$ and a particular functional combination of partial derivatives that ensures the gauge invariance between $j^\mu(x)$ and $A^\mu(x)$. Upon a change of the gauge in $(A^\mu)'(x) \to A^\mu(x) - \partial^\mu\Lambda(x)$ for any local function of $\Lambda(x)$, the gauge invariance of the relationship between $j^\mu(x)$ and $A^\mu(x)$ can be easily demonstrated by direct substitution in Equation (4).

The quark current $j^\mu(x)$ in turn generates a new gauge field $\tilde{A}^\mu(x)$ through the Maxwell equation,

$$\partial_\nu F^{\nu\mu}(x) = \partial_\nu\{\partial^\nu\tilde{A}^\mu(x) - \partial^\mu\tilde{A}^\nu(x)\} = g_{2D}j^\mu(x) = g_{2D}\langle\bar{\psi}(x)\gamma^\mu\psi(x)\rangle. \tag{5}$$

A stable collective particle–hole excitation of the quark system occurs when the initial applied $A^\mu(x)$ gives rise to the induced quark current j^μ, which in turn leads to the new gauge field $\tilde{A}^\mu(x)$ self-consistently. We impose this self-consistency condition of the gauge field, $A^\mu(x) = \tilde{A}^\mu(x)$. In that case, Equations (4) and (5) are mathematically the same as

$$\partial_\nu \partial^\nu A^\mu(x) + \frac{g_{2D}^2}{\pi} A^\mu(x) = 0, \tag{6}$$

and

$$\partial_\nu \partial^\nu j^\mu(x) + \frac{g_{2D}^2}{\pi} j^\mu(x) = 0. \tag{7}$$

We can follow Casher, Kogut, and Susskind [114] and also Coleman et al. [111,112] to introduce a boson field $\phi(x)$ related to the current $j^\mu(x)$ by

$$j^\mu(x) = \epsilon^{\mu\nu}\partial_\nu \phi(x), \tag{8}$$

where $\epsilon^{\mu\nu}$ is the antisymmetric unit tensor with $\epsilon^{01} = \epsilon^{10} = 1$. The boson field ϕ, the quark current j^μ, and the gauge field A^μ are all related to each other, and thus, the boson field $\phi(x)$ also satisfies the Klein–Gordon equation,

$$\partial_\nu \partial^\nu \phi(x) + \frac{g_{2D}^2}{\pi} \phi(x) = 0, \tag{9}$$

with a boson mass given by Equation (1). Hence, a massless quark and a massless antiquark interacting in the QED gauge interaction in (1+1)D form a bound and confined neutral QED meson ϕ with the mass $m = g_{2D}/\sqrt{\pi}$.

The QED-confined meson in (1+1)D can be viewed in two equivalent ways [24,27]. It can be depicted effectively as a QED-confined one-dimensional open string, with a quark and an antiquark confined at the two ends of the open string subject to an effective linear two-body confining interaction. A more basic and physically correct picture depicts the QED meson as the macroscopic manifestation of the collective space-time oscillation of the gauge field $A^\mu(x)$ associated with the microscopic particle–hole excitation of quarks from the Dirac sea. Through the coupling of the gauge field $A^\mu(x)$ to the quarks in the Dirac equation, a space-time variation of the gauge field $A^\mu(x)$ leads to a space-time variation in the quark current $j^\mu(x)$, which in turn determines the space-time variation of the gauge field $A^\mu(x)$ through the Maxwell equation [35,36,113]. As a consequence of such a self-consistent coupling, a quantized and locally confined space-time collective variations of the macroscopic QED gauge field $A^\mu(x)$ can sustain themselves indefinitely at the lowest eigenenergy state in a collective motion with a mass [24,27]. From such a viewpoint, a QED meson particle is a quantized collective space-time variation of the quark current field $j^\mu(x)$ or the gauge fields $A^\mu(x)$ in a Wheelerian "particle without particle" description.

3. Generalizing the Schwinger Confinement Mechanism from Quarks in QED in (1+1)D to (QED+QCD) in (1+1)D

Even though QCD is a non-Abelian gauge theory, many features of the lowest-energy QCD mesons, such as quark confinement, meson states, and meson production, mimic those of the Schwinger model for the Abelian gauge theory in (1+1)D as noted early on by Bjorken, Casher, Kogut, and Susskind [114,115]. Such a generic Abelian string feature in hadrons was first recognized even earlier by Nambu [116,117] and Goto [118]. They indicated that in matters of confinement, quark–antiquark bound states, and hadron production of the lowest-energy states, an Abelian approximation of the non-Abelian QCD theory is a reasonable concept. Furthermore, t'Hooft showed that in a system of quarks interacting in the SU($N_{\rm color}$) gauge interaction approximated as a U($N_{\rm color}$) interaction in the large $N_{\rm color}$ limit, planar Feynman diagrams with quarks at the edges dominate, and the QCD dynamics in (3+1)D can be well approximated as an open-string in QCD dynamics in (1+1)D [119,120]. Numerical lattice calculations for a quark and antiquark system exhibit a flux tube structure [121–123], and a flux tube can be idealized as a structureless string in (1+1)D. Thus, the idealization of QCD meson in (3+1)D as an QCD open string in (1+1)D is a reasonable concept.

We wish to adopt here the quasi-Abelian approximation of non-Abelian QCD to obtain stable lowest-energy collective excitations of the QCD gauge fields and quark currents as carried out in [24,27]. We note first that because quarks carry three colors, the current $j^\mu(x)$

and the gauge field A^μ are each a 3×3 matrix with nine matrix elements. They can be naturally separated out into the color-singlet component with the generator t^0,

$$t^0 = \frac{1}{\sqrt{6}} \begin{pmatrix} 1 & 0 & 0 \\ 0 & 1 & 0 \\ 0 & 0 & 1 \end{pmatrix}, \tag{10}$$

and the color-octet components with the eight Gell-Mann generators $t^1, t^2, t^3, ..., t^8$. The nine generators satisfy the orthogonality condition: $2\text{tr}\,(t^i t^j) = \delta^{ij}$, with $i, j = 0, 1, ..., 8$. The quark current and gauge field in the color space can be represented by

$$j_i^\mu(x) = \sum_{i=0}^{8} j_i^\mu(x) t^i, \tag{11a}$$

$$A_i^\mu(x) = \sum_{i=0}^{8} A_i^\mu(x) t^i. \tag{11b}$$

A stable collective oscillation of the quark–QED–QCD system is a localized periodic oscillation of the nine dynamical components $j_i^\mu(x)$ and the associated gauge field $A_i^\mu(x)$. Because the color-singlet current generates only color-singlet QED gauge field, whereas the color-octet current generates only color-octet QCD gauge fields, the color-singlet and color-octet currents and gauge fields give rise to independent collective oscillations.

For the QCD dynamics of the color-octet quark current and gauge field in (1+1)D, we envisage that a stable QCD state leads to a periodic trajectory in the eight-dimensional $t^1, t^2, ..., t^8$ color-octet space. Excitations with a change of the orientation in the state vector in the eight-dimensional color generator space will lead to states that depend on the angular variables in the color generator space, and they represent color excitations which lie substantially above the lowest-energy QCD states. In contrast, the trajectories of the lowest QCD energy states are expected to consist of a variation of the amplitudes of the current and gauge fields, without the variation of the orientation of the trajectory in the eight-dimensional color-octet space. Therefore, with the limited goal of calculating the lowest-energy QCD states, it suffices to consider QCD dynamics of quarks and gauge fields with the trajectory in an arbitrary and fixed orientation in the color generator space, and to allow only the amplitude of the current and gauge field to vary.

By projecting the eight-dimensional color generator space onto a single arbitrary color generator axis and limiting the dynamics along that direction, we attain the quasi-Abelian approximation which is a reasonable approximation for the lowest QCD states that do not involve gluon excitations. The Nambu–Goto string [116–118] is an Abelian string, and it provides an adequate description of the lowest QCD states. Casher, Kogut and Susskind [114] used the Schwinger Abelian open string as a good model for particle production in the fragmentation of a quark–antiquark pair. The Yo-Yo model of hadrons [124] in the Lund Model [125] used the Abelian strings to describe hadron bound states. Phenomenological non-relativistic and relativistic quark models for the investigation of the low-lying spectrum can remain useful by limiting themselves to dynamics without the color excitation in the quasi-Abelian approximation.

Among the eight generators in the color-octet generator space, t^1 is just as randomly and arbitrarily oriented as any other color-octet generator. The generator t^1 can be taken as a generic generator for the color-octet sector. We therefore represent the QCD current and gauge fields by the $j_1^\mu(x)t^1$ and $A_1^\mu(x)t^1$ along only the t^1 direction. Because t^1 commutes with itself, the dynamics of the current and gauge fields in QCD with the t^1 generator is Abelian. Fixing the orientation of the generator vector t^1 as unchanged is a quasi-Abelian approximation of the non-Abelian QCD dynamics in a subspace, in which the dynamics of the quark-QCD systems can lead to stable QCD collective excitations of the lowest-energy states.

Upon including (i) the above QCD current $j_1^\mu(x)$ and gauge field A_1^μ associated with the color-octet SU(3) generator t^1 to describe the quasi-Abelian QCD dynamics as in [24,27],

and also (ii) the QED current $j_0^\mu(x)$ and gauge field A_0^μ associated with the color-singlet U(1) generator t^0 to describe the QED dynamics of the color-singlet component, we have the sum current and gauge field

$$j^\mu(x) = j_0^\mu(x)t^0 + j_1^\mu(x)t^1, \tag{12a}$$

$$A^\mu(x) = A_0^\mu(x)t^0 + A_1^\mu(x)t^1, \tag{12b}$$

where the generators t^0 and t^1 satisfy $2\mathrm{tr}(t^\lambda t^{\lambda'}) = \delta^{\lambda\lambda'}$, with $\lambda, \lambda' = 0, 1$. Subject to the above applied disturbing gauge field $A^\mu(x)$ with both the QED and the QCD interactions within the quasi-Abelian approximation in (1+1)D, the massless quark field $\psi(x)$ satisfies the Dirac equation,

$$\gamma_\mu(p^\mu - \sum_{\lambda=0}^{1} g_{2D}^\lambda A_\lambda^\mu t^\lambda)\psi = 0, \tag{13}$$

where the quark field ψ is a column vector in color space, and $\lambda = 0$ for the QED interaction, and $\lambda = 1$ for the QCD interaction. The massless quark field leads to the gauge-invariant induced quark current $j_\lambda^\mu(x) = 2\mathrm{tr}\langle\bar{\psi}(x)\gamma^\mu t^\lambda\psi(x)\rangle$ which can be evaluated and found to relate explicitly to the applied QED gauge field $A^\mu(x)$ by [24,27,33]

$$j_\lambda^\mu(x) = -\frac{g_{2D}^\lambda}{\pi}\left(A_\lambda^\mu(x) - \partial^\mu\frac{1}{\partial_\eta\partial^\eta}\partial_\nu A_\lambda^\nu(x)\right), \quad \lambda = 0 \text{ for QED, and } \lambda = 1 \text{ for QCD.} \tag{14}$$

The induced current j_λ^μ generates a gauge field $\tilde{A}_\lambda^\mu(x)$ through the Maxwell equation,

$$\partial_\nu F_\lambda^{\nu\mu}(x) = \partial_\nu\{\partial^\nu\tilde{A}_\lambda^\mu(x) - \partial^\mu\tilde{A}_\lambda^\nu(x)\} = g_{2D}^\lambda j_\lambda^\mu(x). \tag{15}$$

A stable collective particle–hole excitation of the quark system occurs when the initial applied gauge field $A_\lambda^\mu(x)$ gives rise to the induced quark current j_λ^μ, which in turn leads to the new gauge field $\tilde{A}_\lambda^\mu(x)$ self-consistently. We impose this self-consistency condition for the gauge field, $A_\lambda^\mu(x) = \tilde{A}_\lambda^\mu(x)$. In that case, Equations (14) and (15) are the same as

$$\partial_\nu\partial^\nu A_\lambda^\mu(x) + \frac{(g_{2D}^\lambda)^2}{\pi}A_\lambda^\mu(x) = 0, \tag{16}$$

and

$$\partial_\nu\partial^\nu j_\lambda^\mu(x) + \frac{(g_{2D}^\lambda)^2}{\pi}j_\lambda^\mu(x) = 0, \tag{17}$$

where both $j_\lambda^\mu(x)$ and $A_\lambda^\mu(x)$ satisfy the Klein–Gordon equation for a bound and confined boson with a mass $m^\lambda = g_{2D}^\lambda/\sqrt{\pi}$ given by

$$m^\lambda = \frac{g_{2D}^\lambda}{\sqrt{\pi}}. \tag{18}$$

From the above analysis, we find that the QED and the QCD interactions separate out as independent interactions, and they contain independent collective oscillations of the color-singlet current and the color-octet current, with different oscillation energies proportional to the different coupling constants of the interactions. Such a separation is possible because the relation between j^μ and A^μ as given by Equations (14) and (15) are linear in form but the differential operator in the second term of Equation (14) contains non-trivial and non-linear differential elements, which lead to a self-confined local current that can execute stable collective dynamics of QED and QCD mesons in (1+1)D.

4. Do the QED and QCD Mesons in (1+1)D Represent Physical Mesons in (3+1)D?

From the results in the last section, we know that there can be stable collective QED and QCD meson states in (1+1)D whose masses depend on the coupling constants. They represent different excitations of the quark–QED–QCD medium and can be alternatively

depicted as open-string QED and QCD states in (1+1)D, with the quark and the antiquark at the two ends of the string.

Can these open-string meson states in (1+1)D be the idealization of physical QCD and QED mesons in (3+1)D? An open-string QCD meson in (1+1)D as the idealization of a physical QCD meson in (3+1)D is a generally accepted concept, as discussed in the last section. The observations of the anomalous soft photons, the hypothetical X17 particle, and the hypothetical E38 particle suggest it useful to study the possibility that the QED mesons in (1+1)D may represent physical mesons in the physical world of (3+1)D, just as the QCD mesons.

We shall therefore consider the phenomenological open-string model of QCD and QED mesons in (1+1)D and study whether they may represent physical mesons in (3+1)D by comparing theoretical predictions of the model with experiments.

We note that in (3+1)D, the flux tube has a structure with a transverse radius R_T and the coupling constant g_{4D} is dimensionless. In (1+1)D, however, the open string has no structure, but the coupling constant g_{2D} acquires the dimension of a mass. In an earlier work [126], when we compactify a system with a flux tube in (3+1)D with cylindrical symmetry into a (1+1)D system of a string without a structure, we find that the Dirac equation of for quarks in (3+1)D can be separated into the coupling of the longitudinal and the transverse degrees of freedom. Upon quantizing the transverse degree of freedom to obtain the lowest transverse eigenstates, the longitudinal Dirac equation in (1+1)D contains an effective transverse mass, and a modified coupling constant g_{2D} which depends on the coupling constant g_{4D} in (3+1)D multiplied by the absolute square of the transverse wave function. As a consequence, the longitudinal equation in (1+1)D contains a coupling constant in (1+1)D that encodes the information of the flux tube transverse radius R_T and the coupling constant in (3+1)D in Equation (34) of [126] as

$$(g_{2D})^2 = \frac{1}{\pi R_T^2}(g_{4D})^2 = \frac{4\alpha_{4D}}{R_T^2}, \tag{19}$$

whose qualitative consistency can be checked by dimensional analysis and by subsequent theoretical studies in Appendix B of [33]. The compactification from four-dimensional space-time with cylindrical symmetry to two-dimensional with supplementary transverse degrees of freedom has also been examined from the action principle viewpoint, and the relation Equation (19) relating the coupling constant for the longitudinal system in 2D with the coupling in 4D has also been found valid from the viewpoint of the action integral [33,127].

We can give here a simplified derivation of the above Equation (19). We consider only the (x^0, x^3) degrees of freedom after the separation of the transverse degree of freedom, and we take the Coulomb gauge, $A^3 = 0$. The Maxwell equation for the gauge field A^0_{4D} in (3+1)D involves the 4D coupling constant g_{4D} and the density j^0_{4D} given by

$$\partial_3^2 A^0_{4D} = g_{4D} j^0_{4D}. \tag{20}$$

In the compactified (1+1)D string picture, there is a similar Maxwell equation involving A^0_{2D}, the 2D coupling constant g_{2D}, and the density j^0_{2D}, given by

$$\partial_3^2 A^0_{2D} = g_{2D} j^0_{2D}. \tag{21}$$

The (3+1)D charge density j^0_{4D} and the (1+1)D charge density j^0_{2D} are related by

$$j^0_{4D} = \frac{1}{\pi R_T^2} j^0_{2D}. \tag{22}$$

When we compactify the Dirac equation for the quark from (3+1)D to (1+1)D, we identify the gauge interaction term $g_{4D}A^0_{4D}$ in (3+1)D as $g_{2D}A^0_{2D}$ in (1+1)D [33,126]. That is, we have

$$g_{4D}A^0_{4D} = g_{2D}A^0_{2D}. \tag{23}$$

The consistent solution of the above four Equations (20)–(23) leads to the relation between the coupling constants g_{2D} in (1+1)D and g_{4D} in (3+1)D in Equation (19).

With a flux tube in (3+1)D idealized as a string in (1+1)D, the string in (1+1)D can be decoded back to the original physical flux tube in (3+1)D by using the above Equation (19). The boson mass m determined in (1+1)D is the physical mass related to the physical coupling constant $\alpha_{4D}=(g_{4D})^2/4\pi$ and the flux tube radius R_T in (3+1)D by [24]

$$m^2 = \frac{4\alpha_{4D}}{\pi R_T^2}. \tag{24}$$

With $\alpha^{QED}_{4D}=\alpha_{QED}=1/137$, $\alpha^{QCD}_{4D}=\alpha_s\sim 0.6$ from hadron spectroscopy [128–132], and $R_T\sim 0.4$ fm from lattice QCD calculations [133] and $\langle p_T^2\rangle$ of produced hadrons in high-energy e^+e^- annihilations [134], we estimate the masses of the open-string QCD and QCD mesons to be

$$m^{QCD} \sim 431 \text{ MeV}, \quad \text{and} \quad m^{QED} \sim 47 \text{ MeV}. \tag{25}$$

The above mass scales provide an encouraging guide for the present task of a quantitative description of the QCD and QED mesons as open strings, using QCD and QED gauge field theories in (1+ 1)D.

5. Phenomenological Open-String Model of QCD and QED Mesons

For a more quantitative comparison with experimental QCD and QED meson masses, we need an open-string model of QED and QCD mesons with many flavors, and the dependencies of quark attributes on flavors and interactions. By the method of bonsonization, local charge-zero bilinear operator in the Dirac theory corresponds to some local function in the boson theory. The time-like component of the current j^0 for quarks with N_f flavors is [27,112,135]

$$j^0 = \sum_f^{N_f} Q_f :\bar{\psi}_f\gamma^0\psi_f: = \frac{\epsilon^{\mu\nu}}{\sqrt{\pi}}\sum_f^{N_f} Q_f\,\partial_\nu\phi_f, \tag{26}$$

where ϕ_f is the $|q_f\bar{q}_f\rangle$ boson state with the f flavor, Q_f is the charge number for the quark with the f flavor, $Q_u^{QCD} = Q_d^{QCD} = Q_s^{QCD}$ for QCD, and $Q_u^{QED} = \frac{2}{3}$, and $Q_d^{QED} = -\frac{1}{3}$ for QED. The interaction Hamiltonian for the case of massless quarks with N_f flavors is [27,112,135]

$$\begin{aligned}\mathcal{H}_{\text{int}} &= \frac{(g_{2D})^2}{2}\int dx\,dy j^0(x)j^0(y)|x-y| \\ &= \frac{(g_{2D})^2}{2\pi}(\sum_{f=1}^{N_f} Q_f\phi_f)^2.\end{aligned} \tag{27}$$

The physical meson state Φ_i is a flavor mixture D_{ij} of the flavor states ϕ_f,

$$\Phi_i = \sum_{f=1}^{N_f} D_{if}\phi_f, \quad i = 0,...,i_{\max}, \text{ and } i_{\max} = N_f. \tag{28}$$

The inverse transformation is

$$\phi_f = \sum_{i=0}^{i_{\max}}(D^{-1})_{fi}\Phi_i = \sum_{i=0}^{i_{\max}} D_{if}\Phi_i. \tag{29}$$

For massless quarks, the interaction Hamiltonian written in terms of the physical states Φ_i is

$$\mathcal{H}_{\rm int} = \frac{(g_{\rm 2D})^2}{2\pi}(\sum_{f=1}^{N_f} Q_f \sum_{i=0}^{i_{\rm max}} D_{if}\Phi_i)^2. \tag{30}$$

The boson mass square of the physical meson Φ_i is, therefore,

$$m_i^2 = \frac{\partial^2 \mathcal{H}_{\rm int}}{\partial {\Phi_i}^2} = \frac{(g_{\rm 2D})^2}{\pi}(\sum_{f=1}^{N_f} D_{if}Q_f)^2 = \frac{(g_{\rm 2D})^2}{\pi}(\tilde{Q}_{i,\rm eff})^2, \tag{31}$$

where the effective charge $\tilde{Q}_{i,\rm eff}$ for the physical state i is given by

$$\tilde{Q}_{i,\rm eff} = |\sum_{f=1}^{N_f} D_{if}Q_f|. \tag{32}$$

In the massless quark limit, the meson mass for the λth interaction (with $\lambda = 0$ for QED and $\lambda = 1$ for QCD) is

$$(m_i^\lambda)^2 = \frac{(g_{\rm 2D}^\lambda)^2}{\pi}\left[\sum_f^{N_f} D_{if}^\lambda Q_f^\lambda\right]^2. \tag{33}$$

For light quarks with two flavors and isospin symmetry, the physical isoscalar state Φ_0 with $(I = 0, I_3 = 0)$ and the physical isovector state Φ_1 with $(I = 1, I_3 = 0)$ are given in terms of $|u\bar{u}\rangle$ state ϕ_1 and $|d\bar{d}\rangle$ state ϕ_2 by

$$\Phi_0 = \frac{1}{\sqrt{2}}(\phi_1 + \phi_2), \tag{34a}$$

$$\Phi_1 = \frac{1}{\sqrt{2}}(\phi_1 - \phi_2), \tag{34b}$$

$$\text{and} \qquad m_i^\lambda = \frac{g_{\rm 2D}^\lambda}{\sqrt{\pi}}\left|\sum_f^{N_f} D_{if}^\lambda Q_f^\lambda\right| = \frac{g_{\rm 2D}^\lambda}{\sqrt{\pi}}\frac{|Q_u^\lambda - (-1)^i Q_d^\lambda|}{\sqrt{2}}, \quad \text{for isospin } i = 0, 1. \tag{35}$$

For the QCD isovector pion state Φ_1, the effective color charge is $Q_{1,\rm eff}^{\rm QCD}$=$|\sum_{f=1}^2 (D_{1f}Q_f)|$ =$|1/\sqrt{2} - 1/\sqrt{2}|$=0. In the massless quark limit, the above mass formula (35) gives a zero pion mass in Table 1, which is consistent with the common perception in QCD that π^0 is a Goldstone boson. The mass of π^0 comes only from the quark mass and chiral condensate which contribute $\sum_{f=1}^2 m_f\langle\bar{\psi}_f\psi_f\rangle$ to the Lagrangian density and to the π^0 mass square [27,33]

$$\begin{aligned} m_\pi^2 &= \sum_{f=1}^{2} m_f (D_{If}^{\rm QCD})^2 \langle\bar{\psi}_f\psi_f\rangle_{\rm QCD}, \\ &= m_{ud}\langle\bar{\psi}\psi\rangle_{\rm QCD}, \end{aligned} \tag{36}$$

where m_{ud}=$(m_u + m_d)/2$ and $\langle\bar{\psi}\psi\rangle_{\rm QCD}$ is the chiral condensate.

The above equation is consistent with the Gell–Mann–Oakes–Renner relation [136],

$$m_\pi^2 = (m_u + m_d)\frac{|\langle 0|\bar{q}q|0\rangle|}{F_\pi^2}, \tag{37}$$

where $|\langle 0|\bar{q}q|0\rangle|$ is the light u and d quark–antiquark condensate, and F_π is the pion decay constant. We can use the pion mass m_π to calibrate the chiral condensate $\langle\bar{\psi}\psi\rangle_{\rm QCD}$. Therefore, the masses of neutral QCD mesons are given by

$$m^2_{\lambda I} = \frac{4\alpha_\lambda}{\pi R_T^2}\left[\sum_f D^\lambda_{If} Q^\lambda_f\right]^2 + m^2_\pi \frac{\sum_f m_f (D^\lambda_{If})^2}{m_{ud}}, \tag{38}$$

For QCD mesons, Equation (25) indicates that the mass scale $m^{\rm QCD}\sim$ 431 MeV $\gg m_u, m_d, m_s$. It is necessary to include u, d, and s quarks with N_f=3 in the analysis of open-string QCD mesons. We denote $\phi_1 = |u\bar{u}\rangle$, $\phi_2 = |d\bar{d}\rangle$, and $\phi_3 = |s\bar{s}\rangle$, and assume the standard quark model description of $|\pi^0\rangle$, $|\eta\rangle$, and $|\eta'\rangle$ in terms of flavor octet and flavor singlet states, with the mixing of the $|\eta\rangle$ and $|\eta'\rangle$ represented by a mixing angle θ_P [109]. The physical states of $|\pi^0\rangle$, $|\eta\rangle$, and $|\eta'\rangle$ can be represented in terms of the flavor states ϕ_1, ϕ_2 and ϕ_3 by

$$|\pi^0\rangle = \Phi_1 = \frac{\phi_1 - \phi_2}{\sqrt{2}}, \tag{39a}$$

$$|\eta\rangle = \Phi_2 = |\eta_8\rangle\cos\theta_P - |\eta_0\rangle\sin\theta_P, \tag{39b}$$

$$|\eta'\rangle = \Phi_3 = |\eta_8\rangle\sin\theta_P + |\eta_0\rangle\cos\theta_P, \tag{39c}$$

where

$$|\eta_8\rangle = \frac{\phi_1 + \phi_2 - 2\phi_3}{\sqrt{6}}, \tag{39d}$$

$$|\eta_0\rangle = \frac{\sqrt{2}(\phi_1 + \phi_2 + \phi_3)}{\sqrt{6}}. \tag{39e}$$

The QCD states Φ_i=$\sum_f D^{\rm QCD}_{if}\phi_f$ and the flavor component states ϕ_f are then related by

$$\begin{pmatrix}\Phi_1\\ \Phi_2\\ \Phi_3\end{pmatrix} = \begin{pmatrix} \frac{1}{\sqrt{2}} & -\frac{1}{\sqrt{2}} & 0 \\ \frac{1}{\sqrt{6}}\{\cos\theta_P - \sqrt{2}\,\sin\theta_P\} & \frac{1}{\sqrt{6}}\{\cos\theta_P - \sqrt{2}\,\sin\theta_P\} & \frac{1}{\sqrt{6}}\{-2\cos\theta_P - \sqrt{2}\sin\theta_P\} \\ \frac{1}{\sqrt{6}}\{\sin\theta_P + \sqrt{2}\cos\theta_P\} & \frac{1}{\sqrt{6}}\{\sin\theta_P + \sqrt{2}\cos\theta_P\} & \frac{1}{\sqrt{6}}\{-2\sin\theta_P + \sqrt{2}\cos\theta_P\} \end{pmatrix}\begin{pmatrix}\phi_1\\ \phi_2\\ \phi_3\end{pmatrix},$$

with the inverse relation $\phi_f = \sum_{i=1}^3 D^{\rm QCD}_{if}\Phi_i$,

$$\begin{pmatrix}\phi_1\\ \phi_2\\ \phi_3\end{pmatrix} = \begin{pmatrix} \frac{1}{\sqrt{2}} & \frac{1}{\sqrt{6}}\{\cos\theta_P - \sqrt{2}\,\sin\theta_P\} & \frac{1}{\sqrt{6}}\{\sin\theta_P + \sqrt{2}\,\cos\theta_P\} \\ -\frac{1}{\sqrt{2}} & \frac{1}{\sqrt{6}}\{\cos\theta_P - \sqrt{2}\,\sin\theta_P\} & \frac{1}{\sqrt{6}}\{\sin\theta_P + \sqrt{2}\,\cos\theta_P\} \\ 0 & \frac{1}{\sqrt{6}}\{-2\cos\theta_P - \sqrt{2}\sin\theta_P\} & \frac{1}{\sqrt{6}}\{-2\sin\theta_P + \sqrt{2}\cos\theta_P\} \end{pmatrix}\begin{pmatrix}\Phi_1\\ \Phi_2\\ \Phi_3\end{pmatrix}. \tag{40}$$

For these QCD mesons, there is a wealth of information on the matrix $D^{\rm QCD}_{if}$ that describes the composition of the physical states in terms of the flavor components as represented by the mixing angle θ_P between the flavor octet and flavor singlet components of the SU(3) wave functions in η and η' in (39b) and (39c). The ratio of the strange quark mass to the light u and d quark masses that is needed in the above mass formula is also known. From the tabulation in PDG [109], we find $\theta_P = -24.5^\circ$ and m_s/m_{ud}= $27.3^{+0.7}_{-1.3}$. The only free parameters left in the mass formula (38) are the strong interaction coupling constant $\alpha_s = \alpha^{\rm QCD}_{\rm 4D}$ and the flux tube radius R_T.

For the value of α_s, previous works on the non-perturbative potential models use a value of α_s of the order of 0.4–0.6 in hadron spectroscopy studies [128–132,137]. We find that $\alpha_s = 0.68$ gives a reasonable description of the QCD mesons masses considered. For the value of R_T, lattice gauge calculations with dynamical fermions give a flux tube root-mean-square radius R_T = 0.411 fm for a quark–antiquark separation of 0.95 fm [133]. The experimental value of $\langle p_T^2\rangle$ of produced hadrons ranges from 0.2 to 0.3 GeV^2 for e^+-e^- annihilations at $\sqrt{s}$ from 29 GeV to 90 GeV [134], corresponding to a flux tube radius R_T

$= \hbar/\sqrt{\langle p_T^2 \rangle}$ of 0.36 to 0.44 fm. It is reasonable to consider the flux tube radius parameter to be R_T=0.4 fm. This set of parameters of α_s = 0.68 and R_T = 0.40 fm gives an adequate description of the π^0, η and η' masses as shown in the last column of Table 1.

Table 1. Comparison of experimental and theoretical masses of neutral, I_3 = 0 QCD and QED mesons obtained in the massless quark limit and with the semi-empirical mass formula (38) for QCD mesons and (42) for QED mesons, for α_{4D}^{QED} = 1/137, $\alpha_s = \alpha_{4D}^{QCD}$ = 0.68, and R_T = 0.40 fm.

		I	Experimental Mass (MeV)	Meson Mass in Massless Quark Limit (MeV)	Meson Mass Including Quark Mass and Quark Condensate Contributions (MeV)
QCD meson	π^0	1	134.9	0	134.9 ‡
	η	0	547.9	329.7	498.4
	η'	0	957.8	723.4	948.2
QED meson	isoscalar	0		11.2	17.9
	isovector	1		33.6	36.4
Possible QED meson candidates	X17		$16.70 \pm 0.35 \pm 0.5$ [37]		
	X17		$16.84 \pm 0.16 \pm 0.20$ [38]		
	X17		$17.03 \pm 0.11 \pm 0.20$ [41]		
	X17		16.7 ± 0.47 [45]		
	X17		17.1 ± 0.7 [72]		
	E38		37.38 ± 0.71 [103]		
	E38		40.89 ± 0.91 [103]		
	E38		39.71 ± 0.71 [103]		

‡ Calibration mass.

Having provided an adequate description of the neutral QCD meson masses, we wish to extrapolate to the unknown sector of the QED mesons. We do not know the flux tube radius for the QED mesons. We shall proceed by presuming that the flux tube radius may be an intrinsic property of quarks pending modifications by future experimental data. The chiral condensate depends on the interaction type λ and the coupling constant g_{4D}^{λ}. We note that the chiral current anomaly in the chiral current depends on the coupling constant square, $e^2 = g_{4D}^2$ as given in Equation (19.108) of ref. [138]

$$\partial_\mu j^{\mu 53} = -\frac{e^2}{32\pi}\epsilon^{\alpha\beta\gamma\delta}F_{\alpha\beta}F_{\gamma\delta}, \tag{41}$$

which shows that the degree of non-conservation of the chiral current is proportional to e^2. It is therefore reasonable to infer that the chiral condensate term scales as the coupling constant square as g_{4D}^2 or α_{4D}^{λ}, just as the first term. Hence, we have [27]

$$m_{\lambda I}^2 = \frac{4\alpha_{4D}^{\{QCD,QED\}}}{\pi R_T^2}\left[\sum_{f=1}^{N_f} D_{If}^{\lambda} Q_f^{\lambda}\right]^2 + m_\pi^2 \frac{\alpha_{4D}^{\{QCD,QED\}}}{\alpha_{4D}^{QCD}} \frac{\sum_f^{N_f} m_f (D_{If}^{\lambda})^2}{m_{ud}}. \tag{42}$$

By extrapolating to the QED mesons with α_{4D}^{QED}=1/137, with Q_u=2/3 and Q_d=−1/3, we find an open-string isoscalar $I(J^\pi)$=0(0^-) QED meson state at 17.9 MeV and an isovector $(I(J^\pi)$=1$(0^-), I_3 = 0)$ QED meson state at 36.4 MeV. The predicted masses of the isoscalar and isovector QED mesons in Table 1 are close to the mass of the hypothetical X17 and E38 particles. The open-string description of the QCD and QED mesons may be a reasonable concept and the anomalous X17 [37] and E38 [103] observed recently may be QED mesons. The parent particles of the anomalous soft photons [10] may be QED mesons.

The flux tube radius of the QED meson is a phenomenological parameter. The fact that the same flux tube radius used for QCD-confined mesons can describe also the QED-confined QED mesons, together with the non-observation of fractional charges, may suggest

the possibility that the confinement property and the flux tube radius may be intrinsic properties of the quarks.

It is of interest to note the different ordering of the isoscalar and isovector mesons in QCD and QED. For QCD mesons, because the color charges of u and d quarks are equal, the effective color charge for the isovector QCD meson is zero and the effective color charge for the isoscalar QCD meson is large and non-zero. Consequently, for the QCD mesons, $m_{I=1}^{\mathrm{QCD}} < m_{I=0}^{\mathrm{QCD}}$. However, for the QED mesons, because the electric charges of u and d quarks are opposite in signs and different in magnitudes, the effective electric charge for the isoscalar state is small, while the effective electric charge for the isovector state is relatively large, and we have the ordering $m_{I=1}^{\mathrm{QED}} > m_{I=0}^{\mathrm{QED}}$, which is the opposite of the ordering of the QCD mesons.

6. Production, Decay, and Detection of the QED Mesons

To search for QED mesons, it is necessary to consider the production and the decay of the QED mesons. As composite particles of quarks and antiquarks, they are produced when quark and antiquark pairs at the proper QED meson eigenstate energies are produced. Therefore, we expect QED mesons to accompany the production of QCD mesons in hadron–hadron collisions, e^+e^- annihilations, and the coalescence of quark and antiquarks at the deconfinement-to-confinement phase transitions. Experimentally, anomalous soft photon production indeed accompanies QCD hadron production. The transverse momentum distribution of the anomalous soft photons also suggests the occurrence of QED mesons in these reactions [27,46]. However, the anomalous soft photons provide only indirect evidence because their masses have not been directly measured, and their decay properties not explicitly demonstrated. Possible direct evidence for the QED meson may come from the ATOMKI and HUS observations of the hypothetical X17 particle [37,45] as well as the DUBNA observations of anomalous structures at ∼17 and ∼38 MeV [72].

In ATOMKI and HUS experiments, proton beams at a laboratory energy of 0.5 to 4.0 MeV were used to fuse a proton with ^{3}H, ^{7}Li, and ^{11}B target nuclei to form excited states of ^{4}He, ^{8}Be, and ^{12}C, respectively [37–45,47]. The product nuclei are alpha-conjugate nuclei, and the reactions take place at energies below or just above the Coulomb barrier. The alpha-conjugate nuclei have been so chosen that the compound nuclei produced after proton fusion are highly excited, whereas the compound nuclei ground states are closed-shell nuclei of different shapes with extra stability. In particular, the ^{4}He ground state is a spherical closed-shell nucleus. The ^{8}Be ground state is a prolate closed-shell nucleus with a longitudinal-to-transverse radius ratio of about 2:1. The ^{12}C ground state is an oblate closed-shell nucleus with a longitudinal-to-transverse radius ratio of about 1:2 [139]. There is consequently a large single-particle energy gap between particle states above the closed shell and the hole states at the top of the fermi surface below the closed shell. The captured proton in the proton fusion reaction populates a proton single-particle state above the large closed-shell energy gap, and the proton hole is located at the top of the Fermi surface below the closed shell. The transition of the captured proton from the proton particle state to reach the proton hole state below the closed-shell fermi surface will release the large shell-gap energy that is of the order of about 17–20 MeV. Such a large shell–energy gap may be sufficient to produce a neutral boson if there were to exist such a stable neutral boson particle with the proper energy, quantum numbers, and other conditions appropriate for its production. In the spatial configuration space, the captured proton in the valence orbit is located an an extended distance from the alpha conjugate hole nuclear core to facilitate the possible formation of a flux tube structure between the proton and the nuclear core to favor the production of a $q\bar{q}$ open string.

As an example of a possible QED meson production process in a low-energy p+^{3}H proton fusion reaction at ATOMKI and HUS, we show in Figure 1a the Feynman diagram of the excited state of ^{4}He nucleus, which has been prepared by placing a proton in the stretched-out p state interacting with the ^{3}H core in Figure 1a [37–39]. The de-excitation of the ^{4}He* excited state to the ^{4}He(gs) ground state can occur by the proton emitting a virtual

gluon which fuses with the virtual gluon from the ^{3}H core, leading to the production of a $q\bar{q}$ pair as shown in Figure 1a. If the ^{4}He$^*\rightarrow{}^4$He(gs) de-excitation energy exceeds the mass of a confined QED meson $q\bar{q}$, then a QED meson may be produced in conjunction with the ^{4}He$^*\rightarrow{}^4$He(gs) de-excitation as depicted in Figure 1a.

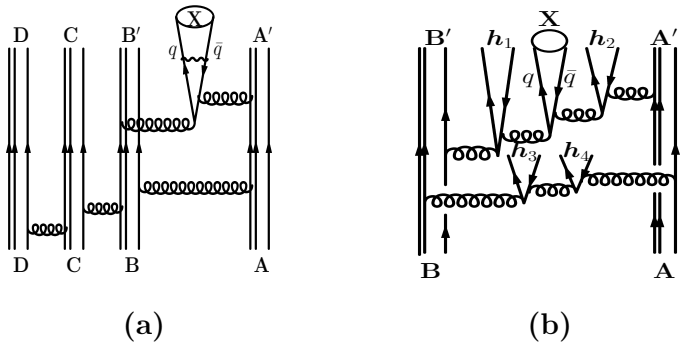

Figure 1. (**a**) $q\bar{q}(X)$ production by the fusion of two virtual gluons in the de-excitation of a highly excited ^{4}He*(ABCD) $\rightarrow{}^4$He (ground state) (A′B′CD) + $q\bar{q}$(X) with the fusion of two virtual gluons between B and A. (**b**) $q\bar{q}(X)$ production in hadron–hadron or a nucleus–nucleus collision by A + B $\rightarrow$ A′ + B′ + $(q\bar{q})^n \rightarrow$ A′ + B′ + $\sum_i h_i + q\bar{q}(X)$.

In the high-energy nucleus–nucleus collision experiments at Dubna [102,103], proton and light ion beams collide with light internal nuclear targets at the JINR Nuclotron at an energy of a few GeV/nucleon, and many $q\bar{q}$ pairs are produced as depicted schematically in Figure 1b,

$$A + B \rightarrow A' + B' + (q\bar{q})^n. \tag{43}$$

The invariant masses of most of the produced $q\bar{q}$ pairs will exceed the pion mass, and they will materialize as QCD mesons, labeled as h_i in Figure 1b. However, there may remain a small fraction of the color-singlet $[q\bar{q}]^1$ pairs with an invariant masses below m_π. The $q\bar{q}$ pairs in this energy range below mass m_π allow the quark and the antiquark to interact non-perturbatively in QED alone, with the QCD interaction as a spectator interaction, to lead to possible QED meson eigenstates labeled schematically as $q\bar{q}(X)$ in Figure 1b.

In other circumstances in the deconfinement-to-confinement phase transition of the quark–gluon plasma in high-energy heavy-ion collisions, a deconfined quarks and a deconfined antiquark in close spatial proximity can coalesce to become a $q\bar{q}$ pair with a pair energy below the pion mass, and they can interact non-perturbatively in QED alone to lead to a possible QED meson if there is QED-confined eigenstate in this energy range.

A QED meson may be detected by its decay products from which its invariant mass can be measured, even though a QED meson in (1+1)D cannot decay, as the quark and the antiquark execute yo-yo motion along the string. In the physical (3+1)D, the structure of the flux tube and the transverse photons must be taken into account, in which case the quark and the antiquark at different transverse coordinates in the flux tube traveling from opposing longitudinal directions in a QED meson can make a turn to the transverse direction, by which the quark and the antiquark can meet and annihilate, leading to the emission of two real transverse photons $\gamma_1\gamma_2$ as depicted in the Feynman diagram Figure 2a. A QED meson can decay into two virtual photons $\gamma_1^*\gamma_2^*$, each of which subsequently decays into an e^+e^- pair as $(e^+e^-)(e^+e^-)$ shown in Figure 2b. The coupling of the transverse photons to an electron pair leads further to the decay of the QED meson into an electron–positron pair e^+e^- as shown in Figure 2c. The mass of a QED meson can be obtained by measuring the invariant mass of its decay products.

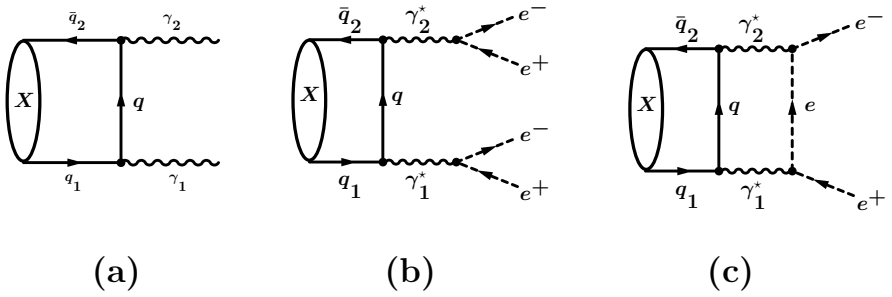

Figure 2. (**a**) A QED meson X can decay into two real photons $X \to \gamma_1 + \gamma_2$. (**b**) It can decay into two virtual photons, each of which subsequently decays into a (e^+e^-) pair, $X \to \gamma_1^* + \gamma_2^* \to (e^+e^-) + (e^+e^-)$, and (**c**) it can decay into a single (e^+e^-) pair, $X \to \gamma_1^* + \gamma_2^* \to e^+e^-$.

7. Experimental Evidence for the Possible Existence of the QED Mesons

7.1. The ATOMKI Observation of the X17 Particle by e^+e^- Measurements

Since 2016, the ATOMKI Collaboration has been observing the occurrence of a neutral boson, the hypothetical X17, with a mass of about 17 MeV, by studying the e^+e^- spectrum in the de-excitation of the excited alpha-conjugate nuclei ^{4}He*, ^{8}Be*, ^{12}C* at various energies in low-energy proton fusion experiments [37,39,41,44]. A summary and update of the ATOMKI results has been presented [43,44], and the confirmation of the ATOMKI data for the $p + ^7$Be reaction by Hanoi University of Science has been reported [45]. Many distribution functions of the opening angle $\theta_{e^+e^-}$ between e^+ and e^- have been successfully described as the production of the X17 particle with an invariant mass of about 17 MeV. The signature for the X17 particle consists of a resonance structure in the invariant mass of the emitted e^+e^- pair. Such a signature is a unique identification of a particle. Because e^+e^- pairs are also produced in many other reaction processes, it is important to subtract contributions from these known processes and from random and cosmic ray backgrounds.

For an optimal detection of the X17 signals, the ATOMKI Collaboration found it necessary to focus on certain regions of the phases space with strong signals so as to enhance the observation probability. For example, in the collision of p with ^{3}H at 0.9 MeV energy, the ATOMKI Collaboration found that the correlation angle $\theta_{e^+e^-}$ of 120° was optimal for a large signal. At such an angle, the energy sum of the e^+ and e^-, $E_{e^+e^-}(\text{sum}) = E_{e^+} + E_{e^-}$ showed a peak structure at around 20.6 MeV as shown in Figure 1 of [39]. Two spectra were constructed for the energy sum $E_{e^+e^-}(\text{sum})$, one at $\theta_{e^+e^-}$=120° and another at 60°, where no X17 signal was expected. The energy sum spectrum in the lower panel of in Figure 1 of ref. [39] was obtained by subtracting the latter from the former, after proper normalization. In the signal region of $19.5 \leq E_{e^+e^-}(\text{sum}) \leq 22.0$ MeV and the background in $5 \leq E_{e+e^-}(\text{sum}) < 19$ MeV, the invariant mass spectrum of the emitted e^+ and e^- showed a resonance structure at $\sim$ 17 MeV as shown in Figure 3.

Previous analysis on the minimum e^+e^- opening angle in X17 decay by Feng et al. [52] supports the validity of the ATOMKI X17 emission model [37]. Similar analysis of the X17 emission to e^+e^- was also carried out by Barducci and Toni [70]. We wish to test here the extended ATOMKI X17 emission model [44], which proposes the emission of the X17 particle not only in the de-excitation of the produced compound nucleus to the ground state but also to an excited state of the compound nucleus [37]. In the ATOMKI emission model, the nature of the X17 and the coupling between the emitting excited alpha conjugate nucleus and the emitted X17 particle are left unspecified. Among many possibilities, the X17 in the model could be the isoscalar QED meson, which has a predicted mass of $\sim$17 MeV and can decay into e^+ and e^- [24,27].

In ATOMKI experiments involving the detection of e^+ and e^-, we envisage that the reaction first goes through the fusion of the projectile nucleus A with the target nucleus B, producing a compound nucleus C^*, which can be either on a resonance or off a resonance among the continuum states. The alpha-conjugate compound nuclei C^* formed by a low-energy proton fusion in the ATOMKI experiments are expected to be essentially simple

shell model states. For example, the lowest ^{4}He* states would have a large component as a proton in the p-shell orbiting a spherical ^{3}H core, while the lowest-energy ^{8}Be* and ^{12}C* states would have large components of an excited ^{4}He* with one and two spectator alpha clusters, respectively. However, more complicated states with other light projectile may also be possible with other light projectiles and light targets at different energies.

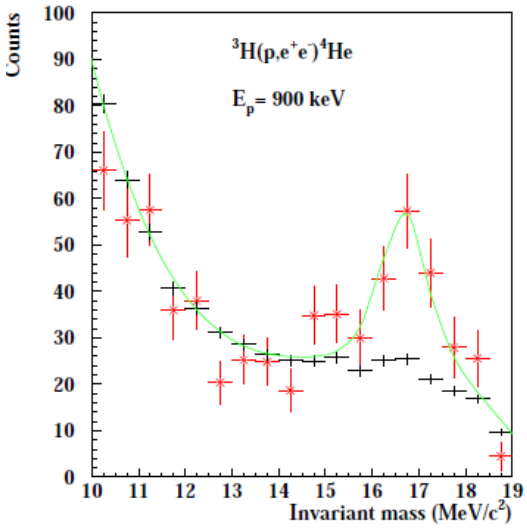

Figure 3. The invariant mass distribution of the emitted e^+ and e^- in the de-excitation of the compound nucleus ^{4}He* state at 20.49 MeV in the ^{3}H$(p, e^+e^-)^4$He$_{gs}$ reaction at $E_p^{lab} = 0.9$ MeV [38]. Red data points are the data in the signal region $19.5 < E_{e^+e^-}(\text{sum}) < 22.0$ MeV, and black points are data in the background region $5 < E_{e^+e^-}(\text{sum}) < 19.0$ MeV. The solid (green) curve is the fit to the invariant mass data points.

The dominant de-excitation of the excited compound nucleus C^* to produce e^+ and e^- is by way of the emission of a photon γ to de-excite radiatively to the compound nucleus C_f state and the conversion of the photon to e^+e^- by internal pair conversion. Here, the C_f state can be an excited state or the ground state C_{gs} of the compound nucleus C. If the final state C_f is an excited state, then there can also be an additional γ_f emission, for example, with $E(\gamma_f) = M(C_f) - M(C_{gs})$. The emitted photon (or photons) can be the source of e^+e^- pairs. By the internal pair conversion process, the emitted photon can be internally converted into an e^+e^- pair,

$$A + B \to C^* \to C_f + \gamma, \quad \text{followed by} \quad \left\{\gamma \xrightarrow{\text{internal conversion}} e^+ + e^- \text{ and } C_f \to C_{gs} + \gamma_f\right\}.$$

The internal pair conversion processes have characteristic e^+e^- angular correlations that depend on the multi-polarity of the $C^* \xrightarrow{\gamma} C_f$ transition. They are relatively smooth distribution functions of the opening angle $\theta_{e^+e^-}$ between e^+ and e^- in the CM system, with no abrupt rises and falls as a function of the opening angle.

In the presence of the internal pair conversion e^+e^- background, the ATOMKI Collaboration searches for an unknown neutral boson X that may be emitted by C^* in its de-excitation to the lower C_f final state or the C_{gs} ground state,

$$A + B \to C^* \to C_f + X, \quad \text{followed by} \quad \left\{X \to e^+ + e^- \text{ and } C_f \to C_{gs} + \gamma_f\right\}. \tag{44}$$

The subsequent decay of the X particle into e^+ and e^- will give the X emission signal in the angular distribution of $\theta_{e^+e^-}$ between e^+ and e^- in ATOMKI-type experiments.

We begin first by studying the X particle decaying into e^+ and e^- in the X rest frame. We denote the four-momenta of e^+ and e^- by $(\epsilon_{e^+}, \vec{p}_{e^+})$ and $(\epsilon_{e^-}, \vec{p}_{e^-})$, respectively. Because

$m_X \gg m_e$, we can neglect the mass of the electron and consider $\epsilon_{e^+} = \epsilon_{e^-} = \frac{m_X}{2} \approx |\vec{p}_{e^+}| = |\vec{p}_{e^-}|$ with $\vec{p}_{e^+}$ pointing in the (θ, ϕ) direction, and $\vec{p}_{e^-} = -\vec{p}_{e^+}$.

To obtain the opening angle $\theta_{e^+e^-}$ in the compound nucleus C^* rest frame, which is also the same as the A+B reaction center-of-mass (CM) frame, we consider next the decay of the compound nucleus C^* to C_f and X. By the decaying process, the X particle acquires a kinetic energy K, and correspondingly, a three-velocity $\vec{\beta}$, which we can take to lie along the z-axis, with $\vec{\beta} = \beta\vec{e}_z$.

To obtain the four-momenta of e^+ and e^- in the CM frame, we boost the four-momenta of e^+ and e^- in the X rest frame by the three-velocity $\vec{\beta}$ of the X particle in the CM system. The three-momenta $\vec{p}'_{e^\pm}$ of the emitted e^+ and e^- in the CM system are therefore

$$\vec{p}'_{e^\pm} = \left\{ \vec{p}_{e^\pm} + \vec{\beta}\gamma\left(\frac{\gamma}{\gamma+1}\vec{\beta}\cdot\vec{p}_{e^\pm} + \epsilon_{e^\pm}\right)\right\}. \tag{45}$$

where $\gamma = 1/\sqrt{1-\beta^2}$. The squares of the energies and the momenta of e^+ and e^- in the CM frame are therefore

$$(\epsilon'_{e^\pm})^2 \approx |\vec{p}'_{e^\pm}|^2 = \left(\frac{m_X}{2}\right)^2 \left\{1 \pm 2\beta\cos\theta\gamma\left(\pm\frac{\gamma}{\gamma+1}\beta\cos\theta + 1\right) + \beta^2\gamma^2\left(\pm\frac{\gamma}{\gamma+1}\beta\cos\theta + 1\right)^2\right\}. \tag{46}$$

where we have used $\vec{\beta}\cdot\vec{p}_{e^+} = \beta|\vec{p}_{e^+}|\cos\theta$. The scalar product of $\vec{p}'_{e^+}$ and $\vec{p}'_{e^-}$ is

$$\begin{aligned}\vec{p}'_{e^+}\cdot\vec{p}'_{e^-} &= |\vec{p}'_{e^+}|\,|\vec{p}'_{e^-}|\cos\theta_{e^+e^-} \\ &= \left(\frac{m_X}{2}\right)^2\left\{\vec{e}_z + \vec{\beta}\gamma\left(\frac{\gamma}{\gamma+1}\beta\cos\theta + 1\right)\right\}\cdot\left\{-\vec{e}_z + \vec{\beta}\gamma\left(-\frac{\gamma}{\gamma+1}\beta\cos\theta + 1\right)\right\}.\end{aligned} \tag{47}$$

The above equations give the relation between the X particle velocity angle θ and the e^+e^- opening angle $\theta_{e^+e^-}$ in the CM frame, from which the distribution of the opening angle in $\theta_{e^+e^-}$ in the CM frame can be obtained, when the distribution function of the X particle velocity angle θ is known.

We can consider the emission of the X particle from the compound nucleus C^* to be isotropic in the CM frame until experimental data provide us with information on the degree of non-isotropy. Even if the X particle may be emitted in a non-zero angular momentum l or when the compound system is captured in an angular momentum l state, the weights of different l_z components may remain equal if there is no preferred target nucleus direction, resulting in an isotropic distribution in the CM system. The isotropic emission corresponds to a distribution of the polar angle θ in the CM frame as

$$\frac{dN}{d\Omega_\theta} = \frac{dN}{d\cos\theta d\phi} = \frac{1}{4\pi}, \tag{48}$$

from which the angular distribution of the opening angle $\theta_{e^+e^-}$ can be obtained as

$$\frac{dN}{d\Omega_{\theta_{e^+e^-}}} = \frac{1}{4\pi}\frac{d\cos\theta}{d\cos\theta_{e^+e^-}}, \tag{49}$$

where the right-hand side can be obtained by using Equations (45)–(47).

We can infer from Equations (46) and (47) that the maximum opening angle in the CM frame between e^+ and e^- occurs when $\vec{\beta}$ is along the z-axis. For such a case, the opening angle between e^+ and e^- is

$$\theta_{e^+e^-}(\max) = \pi. \tag{50}$$

Furthermore, from Equations (46) and (47), the minimum opening angle occurs at $\theta = \frac{\pi}{2}$, which happens when $\vec{\beta}$ is perpendicular to $\vec{p}_{e^+}$ with $\cos\theta = 0$. The minimum opening angle $\theta_{e^+e^-}(\text{min})$ in the CM frame is given by

$$\cos[\theta_{e^+e^-}(\text{min})] = \frac{-1+\beta^2\gamma^2}{1+\beta^2\gamma^2} = -1+2\beta^2, \quad \text{and} \quad \theta_{e^+e^-}(\text{min}) = \cos^{-1}[-1+2\beta^2], \tag{51}$$

as was obtained earlier by Barducci and Toni in ref. [70].

The opening angle between e^+ and e^- in ATOMKI experiments has been measured in the laboratory system. Since the ATOMKI experiments deal with proton reactions with beam energies of only a few MeV, which are much smaller than the proton mass of about 1 GeV, the difference in the opening angles in the laboratory system and the CM system are small. It suffices to compare the opening angle with experimental data measured in the laboratory system with theoretical results calculated in the CM system, using Equation (48), without incurring serious errors.

We study here the minimum opening angles $\theta_{e^+e^-}(\text{min})$ in terms of β^2 and experimental kinematic attributes in different AB fusion collisions so that we can study the emission of the X particle in the de-excitation process, not only to the ground state C_{gs} but also to an excited state C_{f} of the compound nucleus. The quantity β^2 in Equation (51) by

$$\beta^2 = \vec{\beta}^2 = \frac{2K}{m_X}\left[1+\frac{K}{2m_X}\right] \Big/ \left\{1+\frac{2K}{m_X}\left[1+\frac{K}{2m_X}\right]\right\}, \tag{52}$$

where K is the kinetic energy of X and its emission partner C_{f} in the CM frame. The quantity K is given explicitly by

$$K = E_x - [M(C_{\text{f}}) - M(C_{\text{gs}})] - m_X, \tag{53}$$

$$E_x = \frac{AB}{A+B}E_A^{\text{lab}} + Q_{\text{gs}}, \tag{54}$$

$$Q_{\text{gs}} = M(A) + M(B) - M(C_{\text{gs}}), \tag{55}$$

where E_x is the excitation energy of the compound nucleus C^* relative to its ground state C_{gs}; $M(C_{\text{f}})$ and $M(C_{\text{gs}})$ are the masses of the nucleus C at the C_{f} state and the ground state C_{gs}, respectively; Q_{gs} is the Q value of the AB fusion reaction relative to the ground state C_{gs} of the fused compound nucleus C; and $M(A)$ and $M(B)$ are the masses of the projectile and target nucleus A and B with atomic mass numbers A and B, respectively.

The quantity K is the sum of the kinetic energy of X and the kinetic energy of its emission partner C_{f} in the CM system,

$$K = \sqrt{|\vec{p}_X|^2 + m_X^2} - m_X + \frac{|\vec{p}_X|^2}{2M(C_{\text{f}})}. \tag{56}$$

As $M(C_{\text{f}}) \gg m_x$ and $|\vec{p}_X|^2/2m_X \gg |\vec{p}_X|^2/2M(c_{\text{f}})$, the quantity K is essentially the kinetic energy of X in the CM system.

We specialize to ATOMKI experiments, where we have

$$Q_{\text{gs}}(p + {}^3\text{H} \to {}^3\text{He}_{\text{gs}}) = M(p) + M({}^3\text{H}) - M({}^4\text{He}_{\text{gs}}) = 19.815\ \text{MeV}, \tag{57}$$

$$Q_{\text{gs}}(p + {}^7\text{Li} \to {}^8\text{Be}_{\text{gs}}) = M(p) + M({}^7\text{Li}) - M({}^8\text{Be}_{\text{gs}}) = 17.255\ \text{MeV}, \tag{58}$$

$$Q_{\text{gs}}(p + {}^{11}\text{B} \to {}^{12}\text{C}_{\text{gs}}) = M(p) + M({}^{11}\text{B}) - M({}^{12}\text{C}_{\text{gs}}) = 15.957\ \text{MeV}. \tag{59}$$

The X particle can be presumed to be the hypothetical X17 particle or the isoscalar QED meson. While the internal pair conversion contributions to the $\theta_{e^+e^-}$ distribution are smooth functions of $\theta_{e^+e^-}$, the decay of $X17$ into e^+e^- gives a relatively sharp delimiter to allow a reasonable extraction of the experimental $\theta_{e^+e^-}(\text{min})$ data. From the ATOMKI data

in [37,39,41,44], we extract the minimum opening angle $\theta_{e^+e^-}(\min)$ for different combinations of collision targets, energies, and de-excitation possibilities as listed in Table 2.

Table 2. Experimental $\theta_{e^+e^-}$(min) data for different collision targets, energies, and final state possibilities extracted from the ATOMKI data in [37,39,41,44]. Here, E_x is the excitation energy of the compound nucleus C^* relative to the compound nucleus ground state $C_{\rm gs}$, after proton fusion in the $p + A \to C^*$ reaction. The quantity K is the X17 kinetic energy in the center-of-mass system. We use here $m_X = 16.70$ MeV [39] in the evaluation of K.

Reaction	$E_p^{\rm lab}$ (MeV)	Compound Nucleus	E_x (MeV)	K (MeV)	$\theta_{e^-e^+}$ (min) (Degree)
$p + {}^3$H	0.510 [39]	^{4}He*	20.20	3.50 ± 0.5	100 ± 5
	0.610 [39]	^{4}He*	20.27	3.57 ± 0.5	90 ± 5
	0.900 [39]	^{4}He*	20.49	3.79 ± 0.5	96 ± 5
$p + {}^7$Li	1.10 [37,39]	^{8}Be*	18.22	1.52 ± 0.5	130 ± 5
$p + {}^7$Li	4.0 [44]	^{8}Be*	20.76	^{8}Be$^* \to {}^8$Be(gs) + X17 4.06 ± 0.5	110 ± 5
$p + {}^7$Li	4.0 [44]	^{8}Be*	20.76	^{8}Be$^* \to {}^8$Be(2_1^+)(3.03 MeV) + X17 1.03 ± 0.5	136 ± 6
$p + {}^{11}$B	1.50 [41]	^{12}C*	17.33	0.63 ± 0.5	145 ± 3
	1.70 [41]	^{12}C*	17.52	0.82 ± 0.5	144 ± 3
	1.88 [41]	^{12}C*	17.68	0.98 ± 0.5	138 ± 3
	2.10 [41]	^{12}C*	17.88	1.18 ± 0.5	134 ± 3

In the extraction of $\theta_{e^+e^-}$(min) from the experimental ATOMKI data, although there may be some ambiguities and uncertainties, we choose the $\theta_{e^+e^-}(\min)$ value to be the midpoint between a sudden jump in the angular distribution of $\theta_{e^+e^-}$ at the onset of the anomaly. The uncertainty of the value of the kinetic energy K of the X particle in Table 2 comes from the uncertainty of the X17 mass, which is of the order 0.5 MeV, and the uncertainty in the $\theta_{e^+e^-}(\min)$ is taken to be the grid size of the measurement. All final nucleus states $C_{\rm f}$ in Table 2 are implicitly ground states, except when specified explicitly as for the case of $p+{}^7$Li at $E_p^{\rm lab}$ = 4 MeV. The experimental attributes of projectile nucleus, target nucleus, proton collision energies, and final compound nucleus states $C_{\rm f}$ furnish sufficient information to allow the determination of the important physical quantity K, the X17 kinetic energy in the CM frame. To compare the theoretical predictions of the X17 emission model with experimental data, we plot in Figure 3 the minimum opening angle $\theta_{e^+e^-}(\min)$ as a function of K. The theoretical predictions from Equations (51)–(55) are given as the solid curve. One observes that there is a reasonable agreement between the theoretical curve and the data in Figure 4, indicating the validity of the X17 emission model as was first suggested by the ATOMKI Collaboration [37]. The theoretical curve is insensitive to the change of the X17 mass, and the agreement persists when the X17 mass changes from 16.2 MeV to 17.2 MeV as shown in Figure 4.

The minimum opening angle can be used to delimit the region of the e^+e^- phase space relevant for the production of the X17. In the evaluation of the invariant mass of the e^+e^- pair, the $\theta_{e^+e^-}(\min)$ delimiter can be used to exclude contributions of e^+e^- yields with opening angles much less than $\theta_{e^+e^-}(\min)$, which can help eliminate part of the e^+e^- background. It indicates that the X17 kinetic energy variable K in the CM frame is the most important kinematical variable in setting the limit of the opening angle. The correlation of the experimental $\theta_{e^+e^-}(\min)$ with other reaction attributes will provide useful information on the associated likelihood of X17 production. For example, one may ask how $\theta_{e^+e^-}(\min)$ correlates with K, when K is allowed to vary between resonances. Is the resonance with particular quantum numbers essential for the presence or absence of $\theta_{e^+e^-}(\min)$?

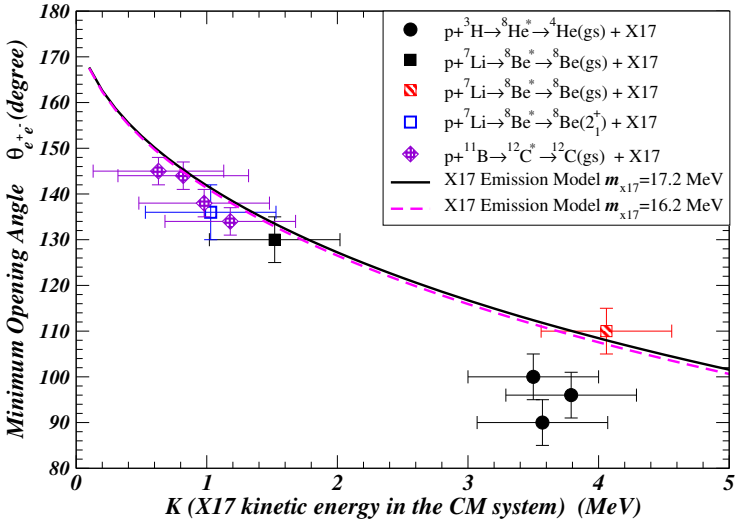

Figure 4. Comparison of the ATOMKI experimental data [37,39,41,44] with the ATOMKI X17 emission model predictions of the minimum opening angle $\theta_{e^+e^-}$(min) between e^+ and e^- as a function of the X17 kinetic energy K in the CM frame, for different collision energies, targets, and final states. The X17 emission model envisages the fusion of the incident proton p with the target nucleus A, forming a compound nucleus C^*, which subsequently de-excites to the final state C_f with the simultaneous emission of the X17 particle. The subsequent decay of the X17 particle into e^+ and e^- then gives the angle $\theta_{e^+e^-}$ between e^+ and e^-. The solid curve is the theoretical prediction of $\theta_{e^+e^-}$(min) as a function of the X17 kinetic energy K, and the ATOMKI data points are from [37,39,41,44] as summarized in Table 2.

ATOMKI reported the observation of the emission of the X17 particle in the de-excitation of the compound nucleus ^{8}Be* to the excited state of ^{8}Be(3.03 MeV) [44]. We show here that the minimum opening angle $\theta_{e^+e^-}$(min) follows the same systematics as other reactions with the X17 emission. The ATOMKI X17 emission model is therefore shown to be valid also for the de-excitation of the compound nucleus C^* to an excited state C_f of the compound nucleus. Such a case occurs at a higher collision energy ($p_p^{\rm lab} = 4$ MeV), leading to the population of a higher compound nucleus state. Such a method of X17 production from a higher excited state C^* to a lower excited state C_f of the compound nucleus opens the door for X17 production at higher fusion collision energies and in fusion reactions using different (projectile A)-(target B) combinations. Furthermore, there is a relatively large X17 yield in the backward angle region near $\theta_{e^+e^-}$=π, where there may be a relatively low competing e^+e^- background. It may provide a way to study the properties of the produced parent X17 particle. It opens up a valuable avenue for future investigation of the X17 particle.

The magnitudes of K in Table 2 provide useful information on the angular momentum carried by the X17 particle when it is emitted simultaneously with its emission partner C_f by the compound nucleus C^* in the CM frame. The quantity K in Table 2 covers a range of only a few MeV. The small magnitude of K suggests that if X is a point particle, then in the emission of X by the compound nucleus C^*, the emission will occur dominantly with X in the S-wave in the CM frame. The emission of X17 carrying $l = 1$ will need to overcome a centrifugal barrier of order $E_l \sim \hbar^2 l(l+1)/2\mu R^2$ where $\mu = m_X m_{C^*}/(m_X + m_{C^*}) \sim m_X$. The barrier E_l is ∼23 MeV even for $R \sim 10$ fm, much greater than the K values in Table 2. On the other hand, if the X particle is a spatially extended object or a wave phenomenon, then the angular momentum may be carried at larger separations outside the nucleus. The spatial nature of the X particle and the angular momentum distribution of the X particle at the moment of emission will need to be investigated. Models of the X emission with non-zero l values will need to be consistent with the small value of the kinetic energy K.

7.2. The Dubna Observation of the X17 and the E38 Particle by Diphoton Measurements

Abraamyan and collaborators at Dubna have been investigating the two-photon decay of particles to study the resonance structure of the lightest hadrons near their thresholds, using d and p beams of a few GeV with fixed internal C and Cu targets at the JINR Nuclotron [72,97,102,103]. Their PHONTON2 detector consists of two arms placed at 26 and 28 degrees from the beam direction, with each arm equipped with 32 lead-glass photon detectors. The photon detectors measure the energies and the emission angles of the photons, from which the invariant masses of the photon pairs can be measured. By selecting photon pairs from the same arm with small opening angles, it is possible to study neutral bosons with small invariant masses, such as those below the pion mass gap m_π. They reported earlier the observation of a resonance structure at a mass of ∼38 MeV [102,103]. In a recent analysis in the diphoton spectrum extended down to the lower invariant mass region, the Dubna Collaboration reported the observation of resonance-like structures both at ∼17 and ∼ 38 MeV in the same experimental setup, in support of the earlier ATOMKI observation of the hypothetical X17 particle and the earlier Dubna observation of the hypothetical E38 particle [72]. The resonance structure of the diphoton signal of the X17 particle appears to be quite strong and prominent as shown in Figure 5.

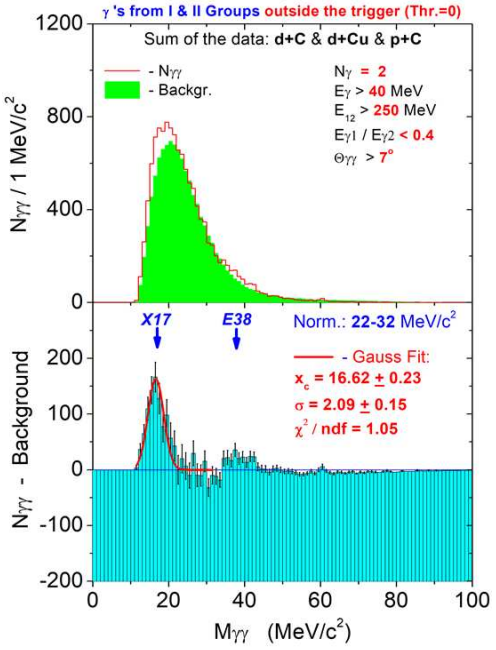

Figure 5. The diphoton invariant mass spectra from light ion collisions with C and Cu targets at a few GeV per nucleon at the JINR Nuclotron, Dubna [72]. The solid curve in the upper panel shows the invariant mass distribution obtained by combining two photons from the same event, and green shaded region the invariant mass distribution by combining two photons from mixed events. The signal of correlated photons subtracting the mixed event background gives the signal represented by the blue region in the lower panel, where the resonance-like structures at ∼17 and ∼38 MeV show up.

The observation of X17 and E38 at Dubna completes an important piece of the anomalous particle puzzle, as the isoscalar X17 and the isovector E38 come in a pair, and they are orthogonal linear combinations of the $|u\bar{u}\rangle$ and $|d\bar{d}\rangle$ components. The agreement of their masses with those predicted by the phenomenological open-string model of QED-confined $q\bar{q}$ model [24,27] lends support to the description that a quark and an antiquark can be confined and bound as stable QED-confined mesons interacting in the Abelian U(1) QED interaction. This is a rather unusual and unfamiliar concept. The confirmation of these anomalous particle observations will be therefore of great interest.

The Dubna observation of the diphoton invariant mass at ∼17 MeV supports the ATOMKI experimental finding of the hypothetical X17 particle using the e^+e^- decay. It sug-

gests further that such a diphoton decay should also occur for the X17 particle produced in ATOMKI-type experiments. In the ATOMKI–Krakow–Munich Collaboration experiments, Nagy et al. search for the diphoton decays of the X17 particle. In the ^{3}H$(p, e^+e^-)^4$He$_{gs}$ experiment using the 2 MV tandem Accelerator of MTA, a proton beam at 1 MeV collides onto a ^{3}H target, and the gamma rays are detected in coincidence with 14 LaBr scintillates. The spectrum of the diphoton energy sums, $dN/dE_{\gamma\gamma}$, from the ^{3}H$(p, \gamma\gamma)^4$He$_{gs}$ reaction, is shown in Figure 6a. In another experiment with the ^{3}He$(n, \gamma\gamma)^4$He$_{gs}$ reaction using the cold neutron beam line of the high-flux reactor at Research Neutron Source of the Technical University of Munich, the Q value of the reaction is 20.6 MeV, so the resonance absorption populates the E_x = 20.21 MeV state as well as the E_x = 21.01 MeV ^{4}He* state using a ^{3}H gas target. The photons are detected in coincidence by an array of 12 scintillators. The spectrum of the diphoton energy sum, $dN/dE_{\gamma\gamma}$, from the ^{3}He$(n, \gamma\gamma)^4$He$_{gs}$ reaction is shown in Figure 6b. As stated in [47] for these measurements, "a peak clearly shows up at 20.6 MeV" in the ^{3}H$(p, \gamma\gamma)^4$He reaction in Figure 6a, but the statistics is, however, poorer.

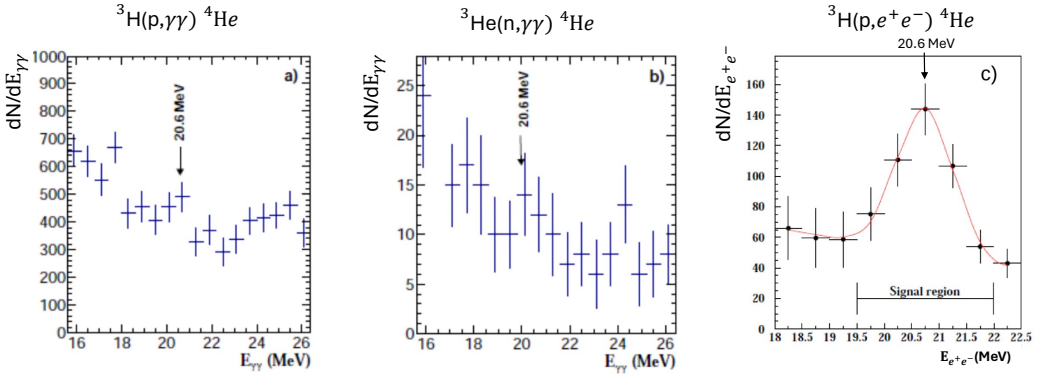

Figure 6. (**a**) The spectrum of the diphoton energy sum, $dN/dE_{\gamma\gamma}$, in the ^{3}H$(p, \gamma\gamma)^4$He$_{gs}$ reaction with a proton beam energy at 1 MeV [47], (**b**) the spectrum of the diphoton energy sum, $dN/dE_{\gamma\gamma}$, in the ^{3}He$(n, \gamma\gamma)^4$He$_{gs}$ reactions using a cold neutron beam line [47], and (**c**) the spectrum of the dilepton energy sum, $dN/dE_{e^+e^-}$, in the ^{3}H$(p, e^+e^-)^4$He$_{gs}$ reaction with a proton beam energy at 0.9 MeV, where the decay of X17 to e^+ and e^- has been observed [39].

It is interesting to compare the spectrum of the diphoton energy sum, $dN/dE_{\gamma\gamma}$, with the spectrum of the dilepton energy sum, $dN/dE_{e^+e^-}$, in Figure 6. The e^+ and e^- particles from the X7 decay have highly relativistic energies, and thus the e^+e^- emission from the X17 dilepton decay follows similar kinematics as the $\gamma\gamma$ emission from the X17 diphoton decay, and vice versa. If X17 decays into e^+e^- and also into $\gamma\gamma$, then $dN/dE_{e^+e^-}$ and $dN/dE_{\gamma\gamma}$ should be very similar for reactions with similar experimental conditions. In Figure 6c, we show $dN/dE_{e^+e^-}$ in the ^{3}H$(p, e^+e^-)^4$He$_{gs}$ reaction with a proton beam of similar energy at 0.9 MeV, where the decay of X17 to e^+ and e^- has been observed. The $dN/dE_{e^+e^-}$ spectrum in Figure 6c exhibits a peak at $E_{e^+e^-}$~20.6 MeV, for which the most likely opening angle $\theta_{e^+e^-}$ is 120^o [39] and corresponds to an invariant mass $m_{e^+e^-}$ of the e^+e^- pair to be

$$(m_{e^+e^-})^2 = 2E_{e^+}E_{e^-}(1-\cos\theta_{e^+e^-}) \sim 2\left(\frac{E_{e^+}+E_{e^-}}{2}\right)^2(1-\cos 120^\circ) = (17.8\ \text{MeV})^2, \quad (60)$$

pointing to the observation of the X17 particle at about 17.8 MeV. The coincidence of the peak position of the spectra for the dilepton energy sum $dN/dE_{e^+e^-}$ in Figure 6c with the peak positions of the spectra for the diphoton energy sum $dN/dE_{\gamma\gamma}$ in Figure 6a,b indicates the likely occurrence of X17 diphoton decay in ATOMKI-type experiments, consistent with the X17 diphoton decay observed by the Dubna Collaboration. The statistics of the peaks in the diphoton energy sum spectra in Figure 6a,b in [47] is, however, poor, and it is important to confirm these diphoton measurements with better statistics to demonstrate the occurrence of X17 diphoton decay in ATOMKI-type experiments.

It is worth noting that the mathematical formulation in the X17 emission model to calculate the opening angle between e^+ and e^- is the same as the formulation to calculate the opening angle between the two photons in the diphoton decay of X17. Consequently, the distribution of the opening angle between the two photons for the X17 diphoton decay would have the same shape as the distribution of the opening angles between e^+ and e^- in the X17 dilepton decay. The dependence of the minimum opening angle between the two photons in the CM system on the X17 kinetic energy K should likewise be the same as that between e^+ and e^-. The extensive set of ATOMKI data on X17 dilepton decay into e^+ and e^- in various reactions may be a useful resource in predicting the behavior for the X17 diphoton decay, which may assist in the design of diphoton measurements in proton fusion experiments.

Possible direct X17 and E38 diphoton decay signals may come from the resonance structure of the diphoton invariant mass at around 15 MeV and 38 MeV in the $pp \rightarrow pp\pi^+\pi^-(\gamma\gamma)$ reaction at $p_{\mathrm{lab}}(p)$= 190 GeV/c [140–144] and the $\pi^- p \rightarrow \pi^- p_{\mathrm{slow}}\pi^+\pi^-(\gamma\gamma)$ reaction at $p_{\mathrm{lab}}(\pi^-)$ = 190 GeV/c, obtained by the COMPASS Collaboration as pointed out by [98–101]. A possible direct signal may also be the prominent resonance structure at 38 MeV in the diphoton invariant mass spectrum in PbPb collisions at $\sqrt{s_{\mathrm{NN}}} = 2.76$ TeV (Figure 5.6 in ref. [145]) obtained by the CMS Collaboration [146].

8. Implications of Quark Confinement in the QED Interaction

8.1. Confinement May Be an Intrinsic Property of Quarks

The observations of the anomalous soft photons, the X17 particle, and the E38 particle provide promising evidence for the possible existence of the QED mesons, which are hypothetical $q\bar{q}$ states confined and bound non-perturbatively by the QED interaction. Their masses at ∼17 and ∼38 MeV are close to the theoretically predicted masses of isoscalar and isovector QED mesons. The occurrence of the isoscalar and isovector doublet reflects properly the two-flavor nature of the light quarks. Their decays into $\gamma\gamma$ and e^+e^- indicate their composite nature and their connection to the QED interaction. Their modes of production by low-energy proton fusion and by high-energy nuclear collisions can also be understood in terms of the production of quark–antiquark pairs by soft gluon fusion or the $(q\bar{q})$ production by string fragmentation in high-energy hadron–hadron collisions [27].

While the confirmation of the observations is pending, it is of interest to examine the implication of the existence of the QED mesons if these observations are indeed confirmed under further scrutiny. It will indicate that the attribute of quark confinement may not be the sole property of the QCD interaction alone and that quarks may also be confined in the QED interaction as QED mesons in the mass region of many tens of MeV. It is possible that the confinement attribute may be an intrinsic property of quarks. Such a possibility is consistent with the observational absence of free quarks or fractional charges. It indicates further that in the multitudes of non-perturbative interactions between a quark and an antiquark, there may be an underlying quark confinement principle which holds that in the dynamics of quarks in different interactions, each interaction always leads to the confinement of quarks. A quark and its antiquark may be confined and bound as a neutral boson in the weak interaction and the gravitational interaction with the exchange of a Z^0 boson or a graviton.

The possibility of quarks being confined in the QED interaction also implies that the QED interaction between a quark and an antiquark may differ from the QED interaction between an electron and a positron. It will be of great interest to inquire what other additional different properties there can be between quarks and electrons and why they are different. For example, the integer electric charge of electrons and fractional electric charges of quarks remain an unresolved problem. There is the question of whether the QED interaction between an electron and a positron may belong to the non-compact non-confining QED theory while the QED interaction between a quark and an antiquark belong to the confining compact QED theory. The possibilities of the compact and non-compact QED bring with them the question whether the QED interaction is unique or is endowed

with a multitude of experimentally testable particle-dependent possibilities with different properties. A related question is whether the QED interaction between quarks in a nucleon may also contain the linear QED confinement component that depends on the magnitudes and signs of the electric charges in addition to the standard Coulomb component.

8.2. QED Meson Assembly and Dark Matter

Astrophysical objects consisting of a large assembly of isoscalar $I(J^\pi) = 0(0^-)$ QED mesons such as the X17 particle with a mass m_X = 17 MeV will be electron–positron emitters, gamma ray emitters, or dark black holes with no emission. The mode of emission, the emission energies, and the lifetimes depend on the gravitational energy of the assembly. Such assemblies of QED mesons present themselves as good candidates of e^+e^- emitters, gamma-ray emitters, or the primordial dark matter. We can make estimates on the constraints on masses and radii of such assemblies where they may be found.

If we consider an assembly of A number of m_X QED mesons of mass $M_A \equiv M$ and we place a test QED m_X meson at the surface of the assembly at radius R, the mass M_{A+1} of the combined system is

$$M_{A+1} = M_A + m_X - \frac{GM_A m_X}{Rc^2}, \tag{61}$$

where G is the gravitational constant. The Q value for the test QED meson at the surface of the (A+1) assembly to decay into an electron–positron pair is

$$Q((A+1) \to A + e^+e^-) = m_X c^2 - \frac{GM_A m_X}{R} - 2m_e c^2. \tag{62}$$

The Q value for the test QED meson to decay into two photons is

$$Q((A+1) \to A + 2\gamma) = m_X c^2 - \frac{GM_A m_X}{R}. \tag{63}$$

Thus, the QED meson assembly of mass M and radius R will be an e^+e^- and γ emitter if

$$\frac{M}{R} < \frac{c^2}{G}\left(1 - \frac{2m_e}{m_X}\right). \tag{64}$$

The QED meson assembly will emit only gamma rays but no e^+e^- pairs if

$$\frac{M}{R} > \frac{c^2}{G}\left(1 - \frac{2m_e}{m_X}\right). \tag{65}$$

The QED meson assembly will not emit e^+e^- pairs nor gamma rays, and is a dark assembly of matter if

$$\frac{M}{R} > \frac{c^2}{G}, \tag{66}$$

which is essentially the condition for a QED meson black hole.

As the evolution of the earlier Universe is likely to have passed through the phase of the quark–gluon plasma and quarks are essential constituents of the quark–gluon plasma, low-lying confined quark–antiquark states such as the isoscalar QED meson may play important roles in the states of matter after the phase transition from the quark–gluon deconfined phase to the confined matter phase. Astrophysical objects consisting of a large assembly of QED meson $q\bar{q}$ states may therefore be of interest. It offers a pathway for electron–positron emitter, gamma emitter, and black hole formation through the quark–gluon plasma deconfinement phase that is different from the evolutionary path of black hole formation by way of the baryonic stellar evolution.

8.3. New Family of QED-Confined Particles and Dark QED Neutron

The QED mesons are composite objects with a complex structure. They possess additional degrees of freedom of spin–spin, spin–orbit, collective vibrational and rotational motion, flavor admixture, and molecular excited QED mesons states. For example, we can get some idea of the vibrational states from the spectrum of a stretched string as shown in Figure 7 of [28]. The possibility of adding quarks with different flavors, angular momentum, and spin quantum numbers will add other dimensions to the number of species of the QED-confined $q\bar{q}$ composite particles.

The success of the open-string description of the QCD and QED mesons leads to the search for other neutral quark systems stabilized by the QED interaction between the constituents in the color-singlet subgroup, with the color-octet QCD gauge interaction as a spectator field. Of particular interest is the QED neutron with the d, u, and d quarks [28,29]. They form a color product group of $\mathbf{3} \otimes \mathbf{3} \otimes \mathbf{3} = \mathbf{1} \oplus \mathbf{8} \oplus \mathbf{8} \oplus \mathbf{10}$, which contains a color-singlet subgroup $\mathbf{1}$, where the color-singlet currents and the color-singlet QED gauge fields reside. In the color-singlet d-u-d system with three quarks of different colors, the attractive QED interaction between the u quark and the two d quarks overwhelms the repulsion between the two d quarks to stabilize the QED neutron at an estimated mass of 44.5 MeV [28]. The analogous QED proton has been found to be theoretically unstable because of the stronger repulsion between the two u quarks, and it does not provide a bound state nor a continuum state for the QED neutron to decay onto by way of the weak interaction. Hence, the QED neutron may be stable against the weak interaction. It may have a very long lifetime and may be a good candidate for the dark matter. Because QED mesons and QED neutrons may arise from the coalescence of deconfined quarks during the deconfinement-to-confinement phrase transition in different environments, such as in high-energy heavy-ion collisions, neutron star mergers [147–149], and neutron star cores [150], the search for the QED bound states in various environments will be of great interest.

8.4. Beyond the Confining Interaction of a Quark and an Antiquark in (3+1)D

A quark and an antiquark reside predominately in (1+1)D, in which the interaction between a quark and an antiquark is the linear confining interaction for both QED and quasi-Abelian QCD as discussed in Sections 3 and 4. In the physical (3+1)D space-time, such a linear interaction is only the dominant part of the full interaction between the quark and the antiquark. There will be additional residual interactions arising from the presence of the transverse degrees of freedom. There are also contributions from the spin–spin, spin–orbit, tensor, and other higher-order terms of the Breit interaction [128–130,137].

For a confining string with a string tension σ, Lüscher, [151,152] considered the fluctuations in the transverse direction of the flux tube as a massless bosonic field theory in two dimensions with a classical action, for which the action can be integrated out to lead to a potential between a static quark at $\mathbf{r}_1$ and an antiquark at $\mathbf{r_2}$ in the large string length limit as

$$V(\mathbf{r}_1\mathbf{r}_2) = \sigma|\mathbf{r}_1 - \mathbf{r}_2| + c - \frac{\alpha}{|\mathbf{r}_1 - \mathbf{r}_2|} + O\left(\frac{1}{|\mathbf{r}_1 - \mathbf{r}_2|^2}\right), \tag{67}$$

where α depends on the coupling constant, and c is a constant. These are therefore long-range residual interactions in both the confined QCD and QED mesons. They represent corrections that arise from expanding the potential between a quark and an antiquark in powers of their separation $|\mathbf{r}_1 - \mathbf{r}_2|$. A powerful tool to study the non-perturbative behavior of the interquark potential is the "Effective String Theory", in which the confining tube contains the quark and the antiquark at the two ends [116–118,151–156]. The Nambu–Goto action can be integrated exactly in all geometries that are relevant for lattice gauge theories: the rectangle (Wilson loop) in ref. [157], the cylinder (Polyakov loop correlators) in refs. [158,159], and the torus (dual interfaces) in ref. [160].

For quarks with color charge numbers Q_1^{QCD} and Q_2^{QCD} interacting in the QCD interaction, we can match the above Equation (67) with the Cornell potential [161] and the

phenomenological quark–antiquark potentials in refs. [27,128–130,137]. Upon neglecting the spin–spin, spin–orbit, other higher-order terms, and an unimportant potential constant, we have the linear-plus-color-Coulomb interaction of QCD

$$V^{\rm QCD}(\mathbf{r}_1\mathbf{r}_2) = Q_1^{\rm QCD}Q_2^{\rm QCD}\left[\sigma^{\rm QCD}|\mathbf{r}_1-\mathbf{r}_2| - \frac{\alpha_s}{|\mathbf{r}_1-\mathbf{r}_2|}\right]. \tag{68}$$

The quark and the antiquark also interact in the QED interaction. We can generalize the above to include both QCD ($\lambda = 1$) and QED ($\lambda = 0$) interactions to give

$$V(\mathbf{r}_1\mathbf{r}_2) \quad = \sum_{\lambda=0}^{1}(-1)^{\lambda+1}Q_1^\lambda Q_2^\lambda\left[\sigma^\lambda|\mathbf{r}_1-\mathbf{r}_2| - \frac{\alpha_\lambda}{|\mathbf{r}_1-\mathbf{r}_2|}\right]t^\lambda, \quad \lambda = \begin{cases} 0 & \text{QED} \\ 1 & \text{QCD} \end{cases}, \tag{69}$$

where t^0 is the generator of the U(1) gauge subgroup as defined in Equation (10), and t^1 is a fixed generator of the SU(3) subgroup in the eight-dimensional color-octet generator space in the quasi-Abelian approximation of the non-Abelian QCD as discussed in Section 3. The generators t^0 and t^1 satisfy $2\text{tr}(t^\lambda t^{\lambda'}) = \delta^{\lambda\lambda'}$.

The above equation is for a single flavor. In the case with many flavors and flavor mixing, their effects can be taken into account by replacing Q_i^λ by the effective charge $\tilde{Q}_{i,\text{eff}}^\lambda$ of Equation (32). It can be further generalized to the case when the quark constituent and the antiquark constituent possess different flavors. For a composite $q_1\bar{q}_2$ particle with many flavors and flavor mixing, the above interaction between the quark q_q and the antiquark $\bar{q}_2$ becomes

$$V(\mathbf{r}_1\mathbf{r}_2) \quad = \sum_{\lambda=0}^{1}(-1)^{\lambda+1}\tilde{Q}_{q_1}^\lambda \tilde{Q}_{\bar{q}_2}^\lambda\left[\sigma^\lambda|\mathbf{r}_1-\mathbf{r}_2| - \frac{\alpha_\lambda}{|\mathbf{r}_1-\mathbf{r}_2|}\right]t^\lambda. \tag{70}$$

When there is no flavor mixing as in the case of the charm and the beauty quarks, the effective charge are just those of the standard quark model, with $Q_{\{u,d,c,s,t,b\}}^{\rm QCD}$=1 and $Q_{\{u,c,t\}}^{\rm QED}$=2/3, $Q_{\{d,s,b\}}^{\rm QED}$=−1/3, and $Q_{\bar{q}}^\lambda$=−Q_q^λ.

9. Conclusions and Discussion

It has been observed that anomalous soft photons with transverse momenta of many tens of MeV/c are proportionally produced when hadrons are produced, and are not produced when hadrons are not produced, indicating that the production of hadrons is always accompanied by the production of neutral boson particles with masses in the region of many tens of MeV. Independently, in the search of axions with a mass of many tens of MeV, an anomaly pointing to the production of a hypothetical X17 neutral boson particle with a mass of about 17 MeV has been observed in the decay of ^{4}He, ^{8}Be, and ^{12}C excited states at ATOMKI and also at the Hanoi University of Science. There have been also reported observations of the hypothetical X17 and the hypothetical E38 particle at Dubna and at ∼17 and ∼38 MeV. The occurrence of these anomalies has led to the question of whether quarks may be confined when they interact non-perturbatively in the QED interaction.

A related question is whether there are experimental circumstances in which a quark and an antiquark may be produced and may interact non-perturbatively in QED interaction alone, with the QCD interaction as an unexcited background interaction. We find that in hadron–hadron, AA, e^+e^-, and e^-A collisions, there can be situations in which a quark and an antiquark may be produced with a center-of-mass energy below the pion mass gap m_π for collective QCD excitation, and the quark and its antiquark can interact non-perturbatively in the QED interaction alone, lest their non-perturbative interaction in the QCD interaction endow the pair with a mass greater than or equal to the pion mass. It is therefore worth studying the question of quark confinement in the QED interaction.

On the theoretical side, it is well known that according to the Schwinger confinement mechanism, massless fermions interacting in the Abelian QED gauge interactions in (1+1)D are confined for all strengths of the gauge interaction, as in an open string, leading to a confined and bound neutral boson with a mass proportional to the magnitude of the coupling constant.

We ask next whether we can apply the Schwinger confinement mechanism to light quarks. Light quarks have masses of only a few MeV, and they can be approximated as massless. A quark and an antiquark cannot be isolated, so they reside predominantly in (1+1)D. They can be produced and interact in the QED interaction alone as we discussed above. The conditions under which the Schwinger confinement mechanism can be applied are met when a light quark and a light antiquark are produced and interact nonperturbatively with the QED interaction alone. We can apply the Schwinger mechanism to quarks to infer that a light quark and its antiquark are confined in the QED interaction in (1+1)D.

On questions of quark confinement and QCD bound states, the non-Abelian QCD interaction can also be approximated as a quasi-Abelian interaction. As a consequence, the Schwinger confinement mechanism can be applied to quarks interacting in both the QED interaction and the QCD interaction, leading to confined QED and QCD open-string states in (1+1)D, with the composite boson masses depending on the magnitudes of the QCD and QED coupling constants. Such a viewpoint is consistent with the QCD string description of hadrons in the Nambu [116] and Goto [116] string model, the string fragmentation models of particle production of Bjorken, Casher, Kogut, and Susskind [114], the classical yo-yo string model [124], the Lund model [125], the Abelian projection model [162,163], and the Abelian dominance model [164–166].

In a phenomenological analysis, we inquire whether the phenomenological open-string model of QCD and QED mesons in (1+1)D can be the idealization of a flux tube showing up as a bound and confined physical meson in (3+1)D. In such a phenomenological open-string model, we need an important relationship to ensure that the boson mass calculated in the lower (1+1)D can properly represent the mass of a physical boson in (3+1)D. The open string in (1+1)D can describe a physical meson in (3+1)D if the structure of the flux tube is properly taken into account. This can be achieved by relating the coupling constant in (1+1)D with the coupling constant in (3+1)D and the flux tube radius R_T [24,29,126]. Using such a relationship, we find that that π^0, η, and η' can be adequately described as open-string $q\bar{q}$ QCD mesons. By extrapolating into the $q\bar{q}$ QED sector in which a quark and an antiquark interact with the QED interaction, we find an open-string isoscalar $I(J^\pi)$=0(0^-) QED meson state at 17.9 MeV and an isovector $(I(J^\pi)$=1$(0^-), I_3 = 0)$ QED meson state at 36.4 MeV. The predicted masses of the isoscalar and isovector QED mesons in the open-string model of the QCD and QED mesons are close to the masses of the reported X17 and E38 particles observed recently, making them good candidates for these particles. Further experimental confirmation of the X17 and the E38 particles will shed light on the question of quark confinement for quarks interacting in the Abelian U(1) QED interaction and will have important implications on the basic properties of quarks and their interactions.

Funding: The research was supported in part by UT-Battelle, LLC, under contract DE-AC05-00OR22725 with the US Department of Energy (DOE). The US government retains, and the publisher, by accepting the article for publication, acknowledges that the US government retains, a nonexclusive, paid-up, irrevocable, worldwide license to publish or reproduce the published form of this manuscript, or allow others to do so, for US government purposes. DOE will provide public access to these results of federally sponsored research in accordance with the DOE Public Access Plan (http://energy.gov/downloads/doe-public-access-plan, accessed on 9 February 2024), Oak Ridge, Tennessee 37831, USA.

Data Availability Statement: No new data were created or anlyzed in this study. Date sharing is not applicable to this article.

Acknowledgments: The author wishes to thank A. Koshelkin, I-Yang Lee, Jack Y. Ng, Kh. Abraamyan, H. N. da Luz, Che-Ming Ko, Siu Ah Chin, P. Adsley, Gang Wang, Yunshan Cheng, H. Holme, S. Sorensen, T. Awes, and N. Novitzky for helpful discussions and communications. The research was supported in part by the Division of Nuclear Physics, U.S. Department of Energy under Contract DE-AC05-00OR22725 with UT-Battelle, LLC.

Conflicts of Interest: The author declares no conflict of interest.

Notes

[1] The Author thanks the Referee of this Special Issue of Universe for bringing this to his attention.

References

1. Perepelitsa, V. [The DELPHI Collaboration]. Anomalous soft photons in hadronic decays of Z^0. In Proceedings of the XXXIX International Symposium on Multiparticle Dynamics, Gomel, Belarus, 4–9 September 2009.
2. Chliapnikov, P.V. et al. [Brussels-CERN-Genova-Mons-Nijmegen-Serpukhov Collaboration] Observation of direct soft photon production in $\pi^- p$ interactions at 280 GeV/c. *Phys. Lett. B* **1984**, *141*, 276. [CrossRef]
3. Botterweck, F. et al. [EHS-NA22 Collaboration] Direct soft photon production in $K^+ p$ and $\pi^+ p$ interactions at 250 GeV/c. *Z. Phys. C* **1991**, 51, 541–548. [CrossRef]
4. Banerjee, S. et al. [SOPHIE/WA83 Collaboration] Observation of direct soft photon production in $\pi^- p$ interactions at 280 GeV/c. *Phys. Lett. B* **1993**, 305, 182–186. [CrossRef]
5. Belogianni, A. et al. [WA91 Collaboration]. Confirmation of a soft photon signal in excess of QED expectations in $\pi^- p$ interactions at 280 GeV/c. *Phys. Lett. B* **1997**, *408*, 487–492. [CrossRef]
6. Belogianni, A. et al. [WA102 Collaboration]. Further analysis of a direct soft photon excess in pi- p interactions at 280-GeV/c. *Phys. Lett. B* **2002**, *548*, 122–128. [CrossRef]
7. Belogianni, A. et al. [WA102 Collaboration]. Observation of a soft photon signal in excess of QED expectations in pp interactions. *Phys. Lett. B* **2002**, *548*, 129–139. [CrossRef]
8. Abdallah, J. et al. [DELPHI Collaboration]. Evidence for an excess of soft photons in hadronic decays of Z^0. *Eur. Phys. J. C* **2006**, *47*, 273–294. [CrossRef]
9. Abdallah, J. et al. [DELPHI Collaboration]. Observation of the muon inner bremsstrahlung at LEP1. *Eur. Phys. J. C* **2008**, *57*, 499–514. [CrossRef]
10. Abdallah, J. et al. [DELPHI Collaboration]. Study of the dependence of direct soft photon production on the jet characteristics in hadronic Z^0 decays. *Eur. Phys. J. C* **2010**, *67*, 343–366. [CrossRef]
11. Hove, L.V. Cold quark-gluon plasma and multiparticle production. *Ann. Phys.* **1989** *192*, 66–76. [CrossRef]
12. Lichard, P.; Hove, L.V. The cold quark-gluon plasma as a source of very soft photons in high energy collisions. *Phys. Lett.* **1990**, *245*, 605–608. [CrossRef]
13. Lichard, P. Consistency of data on soft photon production in hadronic interactions. *Phys. Rev. D* **1994**, *50*, 6824. [CrossRef] [PubMed]
14. Kokoulina, E.; Kutov, A.; Nikitin, V. Gluon dominance model and cluster production. *Braz. J. Phys.* **2007**, *37*, 785. [CrossRef]
15. Barshay, S. Anomalous soft photons from a coherent hadronic phase in high-energy collisions. *Phys. Lett. B* **1989**, *227*, 279–284. [CrossRef]
16. Shuryak, E. The soft photon puzzle and pion modification in hadronic matter. *Phys. Lett. B* **1989**, *231*, 175–177. [CrossRef]
17. Balek, V.; Pisutova, N.; Pisut, J. The puzzle of very soft photon production in hadronic Interactions. *Acta. Phys. Pol.* **1990**, *B21*, 149.
18. Czyz, W.; Florkowski, W. Soft photon production in the boost invariant color flux tube model. *Z. Phys.* **1994**, *C61*, 171.
19. Nachtmann, O. Nonperturbative QCD effects in high-energy collisions. *arXiv* **1994**, arXiv:hep-ph/9411345.
20. Lebiedowicz, P.; Nachtmann, O.; Szczurek, A. Soft-photon radiation in high-energy proton-proton collisions within the tensor-Pomeron approach: Bremsstrahlung. *Phys. Rev. D* **2022**, *106*, 034023. [CrossRef]
21. Hatta, Y.; Ueda, T. Soft photon anomaly and gauge/string duality. *Nucl. Phys.* **2010**, *837*, 22–39. [CrossRef]
22. Darbinian, S.M.; Ispirian, K.A.; Margarian, A.T. Unruh radiation of quarks and the soft photon puzzle in hadronic interactions. *Sov. J. Nucl. Phys.* **1991**, *54*, 364.
23. Simonov, Y.A. Di-pion decays of heavy quarkonium in the field correlator method. *Phys. At. Nucl.* **2008**, *71*, 1048–1076. [CrossRef]
24. Wong, C.Y. Anomalous soft photons in hadron production. *Phys. Rev. C* **2010**, *81*, 064903. [CrossRef]
25. Wong, C.Y. Anomalous soft photons associated with hadron production in string fragmentation. *AIP Conf. Proc.* **2011**, *1343*, 447-449.
26. Wong, C.Y. An overview of the anomalous soft photons in hadron production. *Proc. Sci.* **2014**, *192*, 2.
27. Wong, C.Y. Open string QED meson description of the X17 particle and dark matter. *J. High Energ. Phys.* **2020**, *2020*, 165. [CrossRef]
28. Wong, C.Y. On the stability of the open-string QED neutron and dark matter. *Eur. Phys. J. A* **2022**, *58*, 100. [CrossRef]
29. Wong, C.Y. QED mesons, the QED neutron, and the dark matter. *EPJ Web Conf.* **2022**, *259*, 13016. [CrossRef]

30. Wong, C.Y. QED meson description of the X17 and other anomalous particles. In Proceedings of the "Shedding Light on X17" Workshop, Rome, Italy, 6–8 September 2021.
31. Wong, C.Y. On the question of quark confinement in the QED interaction. *Front. Phys.* **2023**, *18*, 64401. [CrossRef]
32. Koshelkin, A.; Wong, C.Y. Dynamics of quarks and gauge fields in the lowest-energy states in QCD and QED. In Proceedings of the 41st International Conference in High Energy Physics, Bologna, Italy, 6–13 July 2022.
33. Wong, C.Y.; Koshelkin, A. Dynamics of quarks and gauge fields in the lowest-energy states in QCD and QED. *Eur. Phys. J. A* **2023**, *59*, 285. [CrossRef]
34. Kharzeev, D.E.; Loshaj, F. Anomalous soft photon production from the induced currents in Dirac sea. *Phys. Rev. D* **2014**, *89*, 074053. [CrossRef]
35. Schwinger, J. Gauge invariance and mass II. *Phys. Rev.* **1962**, *128*, 2425. [CrossRef]
36. Schwinger, J. Gauge theory of vector particles. In *Theoretical Physics: Trieste Lectures*; IAEA: Vienna, Austria, 1963; p. 89.
37. Krasznahorkay, A.J. Csatlos, M.; Csige, L.; Gacsi, Z.; Gulyas, J.; Hunyadi, M.; Kuti, I.; Nyako, B.; Stuhl, L.; Timar, J.; et al. Observation of anomalous internal pair creation in ^{8}Be: A possible indication of a light, neutral boson. *Phys. Rev. Lett.* **2016**, *116*, 042501. [CrossRef] [PubMed]
38. Krasznahorkay, A.J.; Csatlos, M.; Csige, L.; Gulyas, J.; Koszta, M.; Szihalmi, B.; Timar, J.; Firak, D.S.; Nagy, A.; Sas, N.J.; et al. New evidence supporting the existence of the hypothetical X17 particle. *arXiv* **2019**, arXiv:1910.10459.
39. Krasznahorkay, A.J.; Csatlos, M.; Csige, L.; Gulyas, J.; Krasznahorkay, A.; Nyako, B.M.; Rajta, I.; Timar, J.; Vajda, I.; Sas, N.J. New anomaly observed in ^{4}He supports the existence of the hypothetical X17 particle. *Phys. Rev. C* **2021**, *104*, 044003. [CrossRef]
40. Sas, N.J.; Krasznahorkay, A.J.; Csatlos, M.; Gulyas, J.; Kertesz, B.; Krasznahorkay, A.; Molnar, J.; Rajta, I.; Timar, J.; Vajda, I.; et al. Observation of the X17 anomaly in the 7Li(p,e^+e^-)8Be direct proton-capture reaction. *arXiv* **2022**, arXiv:2205.07744.
41. Krasznahorkay, A.J.; Krasznahorkay, A.; Begala, M.; Csatlos, M.; Csige, L.; Gulyas, J.; Krako, A.; Timar, J.; Rajta, I.; Vajda, I.; et al. New anomaly observed in ^{12}C supports the existence and the vector character of the hypothetical X17 boson. *arXiv* **2022**, arXiv:2209.10795.
42. Alves, D.S.M.; Barducci, D.; Cavoto, G.; Darmé, L.; Rose, L.D.; Doria, L.; Feng, J.L.; Frankenthal, A.; Gasparian, A.; Goudzovski, E.; et al. Shedding light on X17: Community report. *Eur. Phys. J. C* **2023**, *83*, 230. [CrossRef]
43. Krasznahorkay, A.J. X17: Status of the experiments on ^{8}Be and ^{4}He. In Proceedings of the "Shedding Light on X17" Workshop, Rome, Italy, 6–8 September 2021.
44. Krasznahorkay, A.J.; Krasznahorkay, A.; Csatlos, M.; Csige, L.; Timar, J.; Begala, M.; Krako, A.; Rajta, I.; Vajda, I. Observation of the X17 anomaly in the decay of the Giant Dipole Resonance of ^{8}Be. In Proceedings of the International Symposium on Multiparticle Dynamics, Gyöngyös, Hungary, 20–26 August 2023. Available online: https://indico.cern.ch/event/1258038/contributions/5538279/ (accessed on 1 January 2024).
45. Tran, T.-A.; Tran T.D.; Krasznahorkay, A.J.; Krasznahorkay, A.; Molnár, J.; Pintye, Z.; Nguyen, A.V.; Nguyen, T.N.; Do, T.K.L.; Bui, T.H.; et al. Checking the ^{8}Be anomaly with a two-arm electron positron pair spectrometer. In Proceedings of the International Symposium on Multiparticle Dynamics, Gyöngyös, Hungary, 20–26 August 2023. Available online: https://indico.cern.ch/event/1258038/contributions/5538280/ (accessed on 1 January 2024).
46. D'yachenko, A.T.; Gromova, E.S. Detection of particles of dark matter from the spectrum of secondary particles in high-energy proton-proton collisions in a thermodynamic model. *J. Phys. Conf. Ser.* **2021**, *2131*, 22. [CrossRef]
47. Nagy, A.; Krasznahorkay, A.J.; Ciemala, M.; Csige, L.; Gacsi, Z.; Hunyadi, M.; Klaus, T.; Kmieck, M.; Maj, A.; Pietralla, N.; et al. Searching for the double γ-decay of the X17 particle. *Nuo. Cim.* **2019**, *42C*, 124.
48. Zhang, X.; Miller, G.A. Can nuclear physics explain the anomaly observed in the internal pair production in the Beryllium-8 nucleus? *Phys. Lett.* **2017**, *773*, 159–165. [CrossRef]
49. Alves, D.S.M.; Weiner, N.J. A viable QCD axion in the MeV mass range. *J. High Energy Phys.* **2018**, *7*, 92. [CrossRef]
50. Feng, J.L.; Fornal, B.; Galon, I.; Gardner, S.; Smolinsky, J.; Tait, T.M.P.; Tanedo, P. Protophobic fifth force interpretation of the observed anomaly in ^{8}Be nuclear transitions. *Phys. Rev. Lett.* **2016**, *117*, 071803. [CrossRef] [PubMed]
51. Feng, J.L.; Fornal, B.; Galon, I.; Gardner, S.; Smolinsky, J.; Tait, T.M.P.; Tanedo, P. Particle physics models for the 17 MeV anomaly in beryllium nuclear decays. *Phys. Rev. D* **2017**, *95*, 035017. [CrossRef]
52. Feng, J.L.; Tait, J.M.P.; Verhaaren, B. Dynamical Evidence For a Fifth Force Explanation of the ATOMKI Nuclear Anomalies. *Phys. Rev. D* **2020**, *102*, 036016. [CrossRef]
53. Batley, J. et al. [NA48/2 Collaboration]. Search for the dark photon in π^0 decays. *Phys. Lett.* **2015**, *178*, B746.
54. Fornal, B. Is there a sign of new physics in beryllium transitions? *Int. J. Mod. Phys. A* **2017**, *32*, 1730020. [CrossRef]
55. Bordes, J.; Chan, H.M.; Tsun, T.S. Accommodating three low-scale anomalies (g-2, Lamb shift, and Atomki) in the framed standard model. *Int. J. Mod. Phys. A* **2019**, *34*, 1830034. [CrossRef]
56. Chan, H.M.; Tsou, S.T. Two variations on the theme of Yang and Mills—The SM and the FSM. *arXiv* **2022**, arXiv:2201.12256.
57. Bordes, J.; Chan, H.M.; Tsun, T.S. Resolving an ambiguity of Higgs couplings in the FSM, greatly improving thereby the model's predictive range and prospects. *Int. J. Mod. Phys. A* **2022**, *37*, 2250167. [CrossRef]
58. Bordes, J.; Chan, H.M.; Tsun, T.S. A vacuum transition in the FSM with a possible new take on the horizon problem in cosmology *Int. J. Mod. Phys. A* **2023**, *38*, 2350124. [CrossRef]
59. Rose, L.D.; Khalil, S.; King, S.J.D.; Moretti, S.; Thabt, A.M. Explanation of the 17 MeV Atomki anomaly in a U(1)-extended two Higgs doublet model. *Phys. Rev. D* **2017**, *96*, 115024. [CrossRef]

60. Rose, L.D.; Khalil, S.; King, S.J.D.; Moretti, S.; Thabt, A.M. Atomki anomaly in family-dependent U(1) extension of the standard model. *Phys. Rev. D* **2019**, *99*, 055022. [CrossRef]
61. Rose, L.D.; Khalil, S.; King, S.J.D.; Moretti, S.; Thabt, A.M. New physics suggested by Atomki anomaly. *Front. Phys.* **2019**, *7*, 73. [CrossRef]
62. Kubarovsky, V.; West, J.R.; Brodsky, S.J. Quantum Chromodynamics Resolution of the ATOMKI Anomaly in 4He Nuclear Transitions. *arXiv* **2022**, arXiv:2206.14441.
63. Ellwanger, U.; Moretti, S. Possible explanation of the electron positron anomaly at 17 MeV in ^{8}Be transitions through a light pseudoscalar. *J. High Energy Phys.* **2016**, *11*, 39. [CrossRef]
64. Banerjee, D. et al. [NA64 Collaboration]. Search for a hypothetical 16.7 MeV gauge boson and dark photons in the NA64 Experiment at CERN. *Phys. Rev. Lett.* **2018**, *120*, 231802. [CrossRef] [PubMed]
65. Banerjee, D. et al. [NA64 Collaboration]. Search for vector mediator of dark matter production in invisible decay mode. *Phys. Rev. D* **2018**, *97*, 072002. [CrossRef]
66. Banerjee, D. et al. [NA64 Collaboration]. Improved limits on a hypothetical X(16.7) boson and a dark photon decaying into e^+e^- pairs. *Phys. Rev. D* **2020**, *101*, 071101. [CrossRef]
67. Taruggi, C. et al. [PADME Collaboration]. Searching for dark photons with the PADME experiment. *Frascati Phys. Ser.* **2018**, *67*, 17–28.
68. Viviani, M.; Girlanda, L.; Kievsky, A.; Marcucci, L.E. n + 3 H, p + 3 He, p + 3 H, and n + 3 He scattering with the hyperspherical harmonic method. *Phys. Rev. C* **2020**, *102*, 034007. [CrossRef]
69. Viviani, M.; Filandri, E.; Girlanda, L.; Gustavino, C.; Kievsky, A.; Marcucci, L.E.; Schiavilla, R. X 17 boson and the 3 H (p, e+ e-) 4 He and 3 He(n, e+ e-) 4 He processes: A theoretical analysis. *Phys. Rev. C* **2022**, *105*, 014001. [CrossRef]
70. Barducci, D.; Toni, C. An updated view on the ATOMKI nuclear anomalies. *J. High Energy Phys.* **2023**, *154*, 1–46. [CrossRef]
71. Varro, S. Proposal for an electromagnetic mass formula for the X17 particle. In Proceedings of the ISMD2023 International Symposium on Multiparticle Dynamics, Gyöngyös, Hungary, 20–26 August 2023. Available online: https://indico.cern.ch/event/1258038/contributions/5538336/ (accessed on 1 January 2024).
72. Abraamyan, K.; Austin, C.; Baznat, M.I.; Gudima, K.K.; Kozhin, M.A.; Reznikov, S.G.; Sorin, A.S. Observation of structures at ∼17 and ∼38 MeV/c2 in the $\gamma\gamma$ invariant mass spectra in pC, dC, and dCu collisions at plab of a few GeV/c per nucleon. In Proceedings of the ISMD2023 International Symposium on Multiparticle Dynamics, Gyöngyös, Hungary, 20–26 August 2023. Available online: https://indico.cern.ch/event/1258038/contributions/5538282/ (accessed on 1 January 2024).
73. Bastin, B.; Kiener, J.; Deloncle, I.; Coc, A.; Pospelov, M.; Mrazek, J.; Lamia, L.; Ackermann, D.; Adsley, P.; Bacri, C.-O.; et al. Investigation of a light Dark Boson existence: The New JEDI project. *EPJ Web Conf.* **2023**, *275*, 01012. [CrossRef]
74. Cheng, Y.S. et al. [STAR Collaboration]. Private communications.
75. Papa, A. X17 search with the MEGII apparatus. In Proceedings of the "Shedding Light on X17" Workshop, Rome, Italy, 6–8 September 2021.
76. Benmansour, H. The X17 search with the MEGII apparatus. In Proceedings of the International Symposium on Multiparticle Dynamics, Gyöngyös, Hungary, 20–26 August 2023. Available online: https://indico.cern.ch/event/1258038/contributions/5538281/ (accessed on 1 January 2024).
77. Maj, K. BSM physics using photon-photon fusion processes in UPC in Pb+Pb collisions with ATLAS. In Proceedings of the International Symposium on Multiparticle Dynamics, Gyöngyös, Hungary, 20–26 August 2023. Available online: https://indico.cern.ch/event/1258038/contributions/5538283/ (accessed on 1 January 2024).
78. Kaczmarska, A. Searches for new physics in the Higgs sector at ATLAS. In Proceedings of the International Symposium on Multiparticle Dynamics, Gyöngyös, Hungary, 20–26 August 2023. Available online: https://indico.cern.ch/event/1258038/contributions/5538334/ (accessed on 1 January 2024).
79. da Luz, H.N. Measurements of Internal Pair Creation with a Time Projection Chamber-based setup. In Proceedings of the "Shedding Light on X17" Workshop, Rome, Italy, 6–8 September 2021.
80. da Luz, H.N. The construction of the X17 spectrometer at CTU in Prague. In Proceedings of the International Symposium on Multiparticle Dynamics, Gyöngyös, Hungary, 20–26 August 2023. Available online: https://indico.cern.ch/event/1258038/contributions/5538285/ (accessed on 1 January 2024).
81. Gustavino, C. The search for 4 He anomaly at n_TOF experiment. In Proceedings of the "Shedding Light on X17" Workshop, Rome, Italy, 6–8 September 2021.
82. Depero, E. X17 in the NA64 experiment. In Proceedings of the "Shedding Light on X17" Workshop, Rome, Italy, 6–8 September 2021.
83. Darmé, L.; Raggi, M.; Nardi, E. X17 production mechanism at accelerators. In Proceedings of the "Shedding Light on X17" Workshop, Rome, Italy, 6–8 September 2021.
84. Goudzovski, E. Search for dark photon in $\pi 0$ decays by NA48/2 at CERN. In Proceedings of the "Shedding Light on X17" Workshop, Rome, Italy, 6–8 September 2021.
85. Perrevoort, A.-K. Prospects for Dark Photon Searches in the Mu3e Experiment. In Proceedings of the "Shedding Light on X17" Workshop, Rome, Italy, 6–8 September 2021.
86. Doria, L. Dark Matter and X17 Searches at MESA 4.4.2 Light Dark Matter. In Proceedings of the "Shedding Light on X17" Workshop, Rome, Italy, 6–8 September 2021.

87. Gasparian, A. A Direct Detection Search for Hidden Sector New Particles in the 3–60 MeV Mass Range. In Proceedings of the "Shedding Light on X17" Workshop, Rome, Italy, 6–8 September 2021.
88. Ahmidouch, A. et al. [JLAB-PAC50 Proposal]. A Direct Detection Search for Hidden Sector New Particles in the 3-60 MeV Mass Range. *arXiv* **2021**, arXiv:2108.13276.
89. Kozhuharov, V. Searching X17 with positrons at PADME. In Proceedings of the "Shedding Light on X17" Workshop, Rome, Italy, 6–8 September 2021.
90. Raggi, M. Search for the resonant X17 boson production in PADME Run III. In Proceedings of the International Symposium on Multiparticle Dynamics, Gyöngyös, Hungary, 20–26 August 2023. Available online: https://indico.cern.ch/event/1258038/contributions/5538332/ (accessed on 1 January 2024).
91. Cline, E. et al. [DarkLight Collaboration]. Searching for New Physics with DarkLight at the ARIEL Electron-Linac. *J. Phys. Conf. Ser.* **2022**, *2391*, 012010. [CrossRef]
92. Navratil, P. ARIEL experiments and theory. *J. Phys. Conf. Ser.* **2022**, *2391*, 012002. [CrossRef]
93. Huang, S. et al. [LUXE Collaboration]. Probing new physics at the LUXE experiment. In Proceedings of the 41st International Conference on High Energy physics—ICHEP2022, Bologna, Italy, 6–13 July 2022.
94. Feng, J. Collider searches for X17 and other light gauge bosons. In Proceedings of the International Symposium on Multiparticle Dynamics, Gyöngyös, Hungary, 20–26 August 2023. Available online: https://indico.cern.ch/event/1258038/contributions/5538331/ (accessed on 1 January 2024).
95. Kibédi, T. Searching for the x17 using magnetic separation. In Proceedings of the International Symposium on Multiparticle Dynamics, Gyöngyös, Hungary, 20–26 August 2023. Available online: https://indico.cern.ch/event/1258038/contributions/5538333/ (accessed on 1 January 2024).
96. Azuelos, G.; Broerman, B.; Bryman, D.; Chen, W.C.; da Luz, H.N.; Doria, L.; Gupta, A.; Hamel, L.; Laurin, M.; Leach, K.; et al. Status of the X17 search in Montreal. *arXiv* **2022**, arXiv:2211.11900v1.
97. Abraamyan, K.H.; Baznat, M.; Friesen, A.; Gudima, K.; Kozhin, M.; Lebedev, S.; Maxim, N.; Nikitin, S.; Ososkov, G.; Reznikov, S.; et al. Resonance structure in the $\gamma\gamma$ invariant mass spectrum in pC and dC interactions. *Phys. Rev. C* **2009**, *80*, 034001. [CrossRef]
98. van Beveren, E.; Rupp, G. First indications of the existence of a 38 MeV light scalar boson. *arXiv* **2011**, arXiv:1102.1863.
99. van Beveren, E.; Rupp, G. Material evidence of a 38 MeV boson. *arXiv* **2012**, arXiv:1202.1739.
100. van Beveren, E.; Rupp, G. Reply to Comment on "Material evidence of a 38 MeV boson". *arXiv* **2012**, arXiv:1204.3287.
101. van Beveren, E.; Rupp, G. Z0(57) and E(38): Possible surprises in the Standard Model. *Acta Phys. Pol. Proc.* 2020, *accepted for publication*.
102. Abraamyan, K.; Anisimov, A.B.; Baznat, M.I.; Gudima, K.K.; Nazarenko, M.A.; Reznikov, S.G.; Sorin, A.S. Observation of the E(38)-boson. *arXiv* **2012**, arXiv:1208.3829v1.
103. Abraamyan, K.; Austin, C.; Baznat, M.; Gudima, K.; Kozhin, M.; Reznikov, S.; Sorin, A. Check of the structure in photon pairs spectra at the invariant mass of about 38 MeV/c^2. *EPJ Web Conf.* **2019**, *204*, 08004. [CrossRef]
104. Diamantini, M.C.; Trugenberger, C.A.; Vinokur, V.M. Confinement and Asymptotic Freedom with Cooper pairs. *Nat. Comm. Phys.* **2018**, *1*, 77. [CrossRef]
105. Diamantini, M.C.; Gammaitoni, L.; Trugenberger, C.A.; Vinokur, V.M. Vogel-Fulcher-Tamman criticality of 3D superinsulators. *Sci. Rep.* **2018**, *8*, 15718. [CrossRef] [PubMed]
106. Diamantini, M.C.; Postolova, S.V.; Mironov, A.Y.; Gammaitoni, L.; Strunk, C.; Trugenberger, C.A.; M, V. Vinokur Direct probe of the interior of an electric pion in a Cooper pair superinsulator. *Nat. Comm. Phys.* **2020**, *3*, 142.
107. Diamantini, M.C.; Trugenberger, C.A. *Superinsulators: A Toy Realization of QCD in Condensed Matter*; World Scientific: Singapore, 2020.
108. Diamantini, M.C.; Trugenberger, C.A.; Vinokur, V.M. Quantum magnetic monopole condensate. *Nat. Comm. Phys.* **2021**, *4*, 25. [CrossRef]
109. Tanabashi, M. et al. [Particle Data Group 2019]. Review of Particle Physics. *Phys. Rev. D* **2018**, *98*, 030001. [CrossRef]
110. Workman, R.L. et al. [Particle Data Group 2022]. Review of Particle Physics. *Prog. Theor. Exp. Phys.* **2022**, *2022*, 083C01. [CrossRef]
111. Coleman, S.; Jackiw, R.; Suskind, L. Charge shielding and quark confinement in the massive Schwinger model. *Ann. Phys.* **1975**, *93*, 267–275. [CrossRef]
112. Coleman, S. More about the massive Schwinger model. *Ann. Phys.* **1976**, *101*, 239–267. [CrossRef]
113. Wong, C.Y. *Introduction to High-Energy Heavy-Ion Collisions*; World Scientific: Singapore, 1994.
114. Casher, A.; Kogut, J.; Susskind, L. Vacuum polarization and the absence of free quarks. *Phys. Rev. D* **1974**, *10*, 732. [CrossRef]
115. Bjorken, J.D. *Lectures Presented in the 1973 Proceedings of the Summer Institute on Particle Physics*; SLAC: Menlo Park, CA, USA, 1973; SLAC-167.
116. Nambu, Y. Quark model of the factorization of the Veneziano Amplitude. In *Lectures at the Copenhagen Symposium: Symmetry and Quark Models*; Chand, R., Ed.; Gordon and Breach: Philadelphia, PA, USA, 1970; p. 269.
117. Nambu, Y. Strings, monopoles, and gauge fields. *Phys. Rev. D* **1974**, *10*, 4262. [CrossRef]
118. Goto, T. Relativistic quantum mechanics of one-dimensional mechanical continuum and subsidiary condition of dual resonance model. *Prog. Theo. Phys.* **1971**, *46*, 1560–1569. [CrossRef]
119. 't Hooft, G. A planar diagram theory for strong interactions. *Nucl. Phys. B* **1974**, *72*, 461–473. [CrossRef]
120. 't Hooft, G. A two-dimensional model for mesons. *Nucl. Phys. B* **1974**, *75*, 461–470. [CrossRef]

121. Bali, G.S. et al. [SESAM Collaboration] Observation of string breaking in QCD. *Phys. Rev. D* **2005**, *71*, 114513. [CrossRef]
122. Amado, A.; Cardoso, N.; Bicudo, P. Flux tube widening in compact U(1) lattice gauge theory computed at T < Tc with the multilevel method and GPUs. *arXiv* **2013**, arXiv:1309.3859.
123. Cardoso, N.; Cardoso, M.; Bicudo, P. Inside the SU(3) quark-antiquark QCD flux tube: Screening versus quantum widening. *Phys. Rev. D* **2013**, *88*, 054504. [CrossRef]
124. Artru, X.; Mennessier, G. String model and multiproduction. *Nucl. Phys. B* **1974**, *70*, 93–115. [CrossRef]
125. Andersson, B.; Gustafson, G.; Sjostrand, T. A general model for jet fragmentation. *Zeit Phys. C* **1983**, *20*, 317–329. [CrossRef]
126. Wong, C.Y. The Wigner function of produced particles in string fragmentation. *Phys. Rev. C* **2009**, *80*, 054917. [CrossRef]
127. Koshelkin, A.V.; Wong, C.Y. The compactification of QCD4 to QCD2 in a flux tube. *Phys. Rev. D* **2012**, *86*, 125026. [CrossRef]
128. Wong, C.Y.; Swanson, E.S.; Barnes, T. Cross sections for π- and ρ-induced dissociation of J/ψ and ψ'. *Phys. Rev. C* **2000**, *62*, 045201.
129. Wong, C.Y.; Swanson, E.S.; Barnes, T. Heavy quarkonium dissociation cross sections in relativistic heavy-ion collisions. *Phy. Rev. C* **2001**, *65*, 014903. [CrossRef]
130. Crater, H.W.; Yoon, J.; Wong, C.Y. Singularity Structures in Coulomb-Type Potentials in Two Body Dirac Equations of Constraint Dynamics. *Phys. Rev. D* **2009**, *79*, 034011. [CrossRef]
131. Baldicchi, M.; Nesterenko, A.V.; Prosperi, G.M.; Simolo, C. QCD coupling below 1 GeV from quarkonium spectrum. *Phys. Rev. D* **2008**, *77*, 034013. [CrossRef]
132. Deur, A.; Brodsky, S.J.; de Teramond, G.F. The QCD Running Coupling. *Prog. Part. Nucl. Phys.* **2016**, *90*, 1–74. [CrossRef]
133. Cosmai, L.; Cea, P.; Cuteri, F.; Papa, A. Flux tubes in QCD with (2+1) HISQ fermions. In Proceedings of the 4th Annual International Symposium on Lattice Field Theory, Southampton, UK, 24–30 July 2016.
134. Petersen, A. et al. [Mark II Collaboration] Multihadronic events at E_{CM} =29GeV and predictions of QCD models from E_{CM} = 29 GeV to $E_{\mathrm{CM}} = 93GeV$. *Phys. Rev. D* **1988**, *37*, 1. [CrossRef] [PubMed]
135. Nagy, S. Massless fermions in mutiflavor QED. *Phys. Rev. D* **2009**, *79*, 045004. [CrossRef]
136. Gell-Mann, M.; Oakes, R.J.; Renner, B. Behavior of current divergences under SU(3) X SU(3). *Phys. Rev.* **1968**, *175*, 2195. [CrossRef]
137. Barnes, T.; Swanson, E.S. Diagrammatic approach to meson-meson scattering in the nonrelativistic quark potential model. *Phys. Rev. D* **1992**, *46*, 131. [CrossRef] [PubMed]
138. Peskin, M.E.; Schroeder, D.V. *An Introduction to Quantum Field Theory*; Addison-Wesley Publishing Company: Boston, MA, USA, 1995.
139. Wong, C.Y. Shells in a simple anisotropic harmonic oscillator. *Phys. Lett. B* **1970**, *14*, 668–671. [CrossRef]
140. Bernhard, J.; Schonning, K. et al. [COMPASS Collaboration]. Test of OZI violation in vector meson production with COMPASS. *arXiv* **2013**, arXiv:1109.0272v2.
141. Bernhard, J. Exclusive Vector Meson Production in pp Collisions at the COMPASS Experiment. Ph.D. Thesis, University of Mainz, Mainz, Germany, 2014.
142. Schlüter, T. et al. [COMPASS Collaboration]. The exotic $\eta\pi^-$ wave in 190 GeV $\pi^- p \rightarrow \pi^-\eta' p$ at COMPASS. *arXiv* **2011**, arXiv1108.6191v2.
143. Schlüter, T. The $\pi^-\eta$ and and $\pi^-\eta'$ Systems in Exclusive 190 GeV/c $\pi^- p$ Reactions at COMPASS. Ph.D. Thesis, Univ. München, Munich, Germany, 2012.
144. Bernhard, J.; Friedrich, J.M.; Schlüter, T.; Schönning, K. Comment on "Material evidence of a 38 MeV boson". *arXiv* **2012**, arXiv:1204.2349.
145. Snook, B.A. Measurement of the v2 of π^0 Mesons Produced in $\sqrt{s_{\mathrm{NN}}}$=2.76 TeV PbPb Collisions at the Large Hadron Collider. Ph.D. Thesis, Vanderbilt University, Nashville, TN, USA, 2014.
146. Chatrchyan, S. et al. [CMS Collaboration]. Measurement of the azimuthal anisotropy of neutral pions in Pb-Pb collisions at $\sqrt{s_{NN}}$=2.76 TeV. *Phys. Rev. Lett.* **2013**, *110*, 042301. [CrossRef] [PubMed]
147. Bauswein, A.; Bastian, N-.F.; Blaschke, D.; Chatziioannou, K.; Clark, J.A.; Fischer, T.; Oertel, M. Identifying a first-order phase transition in neutron-star mergers through gravitational waves. *Phys. Rev. Lett.* **2019**, *122*, 061102. [CrossRef] [PubMed]
148. Bauswein, A.; Blacker, S.; Vijayan, V.; Stergioulas, N.; Chatziioannou, K.; Clark, J.A.; Bastian, N-.F.; Blaschke, D.B.; Cierniak, M.; Fischer, T. Equation of state constraints from the threshold binary mass for prompt collapse of neutron star mergers. *Phys. Rev. Lett.* **2020**, *125*, 141103. [CrossRef]
149. Weih, L.R.; Hanauske, M.; Rezzolla, L. Postmerger gravitational-wave signatures of phase transitions in binary mergers. *Phys. Rev. Lett.* **2020**, *124*, 171103. [CrossRef] [PubMed]
150. Annala, E.; Gorda, T.; Kurkela, A.; Naettilae, J.; Vuorinen, A. Evidence for quark-matter cores in massive neutron stars. *Nat. Phys.* **2020**, *16*, 907–910. [CrossRef]
151. Lüscher, M. Symmetry Breaking Aspects of the roughening Transition In Gauge Theories. *Nucl. Phys. B* **1981**, *180*, 317–329. [CrossRef]
152. Lüscher, M.; Symanzik, K.; Weisz, P. Anomalies Of The Free Loop Wave Equation In The Wkb Approximation. *Nucl. Phys. B* **1980**, *173*, 365–396. [CrossRef]
153. Polchinski, J.; Strominger, A. Effective string theory. *Phys. Rev. Lett.* **1991**, *67*, 1681. [CrossRef] [PubMed]
154. Hellerman, S.; Maeda, J.; Maltz, J.; Swanson, I. Effective string theory simplified. *J. High Energy Phys.* **2014**, *9*, 183. [CrossRef]
155. Aharony, O.; Komargodski, Z. The Effective Theory of Long Strings. *J. High Energy Phys.* **2013**, *5*, 118. [CrossRef]

156. Bonati, C.; Caselle, M.; Morlacchi, S. The unreasonable effectiveness of effective string theory: The case of the 3d SU(2) Higgs model. *Phys. Rev. D* **2021**, *104*, 054501. [CrossRef]
157. Billo, M.; Caselle, M.; Pellegrini, R. New numerical results and novel effective string predictions for Wilson loops. *J. High Energy Phys.* **2012**, *1*, 104; Erratum in: *J. High Energy Phys.* **2013**, *4*, 97. [CrossRef]
158. Lüscher, M.; Weisz, P. String excitation energies in SU(N) gauge theories beyond the free-string approximation. *J. High Energy Phys.* **2004**, *7*, 14. [CrossRef]
159. Billo, M.; Caselle, M. Polyakov loop correlators from D0-brane interactions in bosonic string theory. *J. High Energy Phys.* **2005**, *507*, 38. [CrossRef]
160. Billo, M.; Caselle, M.; Ferro, L. The partition function of interfaces from the Nambu-Goto effective string theory. *J. High Energy Phys.* **2006**, *602*, 70. [CrossRef]
161. Eichten, E.; Gottfried, K.; Kinoshita, T.; Kogut, J.B.; Lane, K.B.; Yan, T.M. Spectrum of charmed quark-antiquark bound states. *Phys. Rev. Lett.* **1975**, *34*, 369. [CrossRef]
162. t'Hooft, G. Topology of the gauge condition and new confinement phases in non-Abelian gauge theories. *Nucl. Phys. B* **1981**, *190*, 455.
163. Belvedere, L.V.; Swieca, J.A.; Rothe, K.D.; Schroer, B. Generlaized two-dimensional Abelian gauge theories and confinement. *Nucl. Phys. B* **1979**, *153*, 112–140. [CrossRef]
164. Sekido, T.; Ishiguro, K.; Koma, Y.; Mori, Y.; Suzuki, T. Abelian dominance and the dual Meissner effect in local unitary gauges in SU(2) gluodynamics. *Phys. Rev.C* **2007**, *75*, 064906. [CrossRef]
165. Suzuki, T.; Ishiguro, K.; Koma, Y.; Sekido, T. Gauge-independent Abelian mechanism of color confinement in gluodynamics. *Phys. Rev. D* **2008**, *77*, 034502. [CrossRef]
166. Suganuma, H.; Ohata, H. Local correlation among the chiral condensate, monopoles, and color magnetic fields in Abelian projected QCD. *arXiv* **2021**, arXiv:2108.08499.